AGU PUBLICATIONS

JGR

Journal of Geophysical Research: Planets

RESEARCH ARTICLE
10.1002/2016JE005009

Key Points:
- Galileo plasma data show 5 orders of magnitude drop in density and factor 40 increase in ion temperature between 6 and 30 R_J
- Plasma flow is generally azimuthal between 80 and 100% of corotation
- The data do not show significant persistent variations with local time

Supporting Information:
- Supporting Information S1

Correspondence to:
F. Bagenal,
bagenal@lasp.colorado.edu

Citation:
Bagenal, F., R. J. Wilson, S. Siler, W. R. Paterson, and W. S. Kurth (2016), Survey of Galileo plasma observations in Jupiter's plasma sheet, *J. Geophys. Res. Planets*, *121*, 871–894, doi:10.1002/2016JE005009.

Received 6 FEB 2016
Accepted 11 MAY 2016
Accepted article online 13 MAY 2016
Published online 30 MAY 2016

Survey of Galileo plasma observations in Jupiter's plasma sheet

Fran Bagenal[1], Robert J. Wilson[1], Scott Siler[1], William R. Paterson[2], and William S. Kurth[3]

[1]Laboratory of Atmospheric and Space Physics, University of Colorado Boulder, Boulder, Colorado, USA, [2]Goddard Space Flight Center, Greenbelt, Maryland, USA, [3]Department of Physics and Astronomy, University of Iowa, Iowa City, Iowa, USA

Abstract The plasma science (PLS) instrument on the Galileo spacecraft (orbiting Jupiter from December 1995 to September 2003) measured properties of the ions that were trapped in the magnetic field. The PLS data provide a survey of the plasma properties between ~5 and 30 Jupiter radii (R_J) in the equatorial region. We present plasma properties derived via two analysis methods: numerical moments and forward modeling. We find that the density decreases with radial distance by nearly 5 orders of magnitude from ~2 to 3000 cm^{-3} at 6 R_J to ~0.05 cm^{-3} at 30 R_J. The density profile did not show major changes from orbit to orbit, suggesting that the plasma production and transport remained constant within about a factor of 2. The radial profile of ion temperature increased with distance which implied that contrary to the concept of adiabatic cooling on expansion, the plasma heats up as it expands out from Io's orbit (where Ti ~ 60–80 eV) at ~6 R_J to a few keV at 30 R_J. There does not seem to be a long-term, systematic variation in ion temperature with either local time or longitude. This latter finding differs from earlier analysis of Galileo PLS data from a selection of orbits. Further examination of all data from all Galileo orbits suggests that System III variations are transitory on timescales of weeks, consistent with the modeling of Cassini Ultraviolet Imaging Spectrograph observations. The plasma flow is dominated by azimuthal flow that is between 80% and 100% of corotation out to 25 R_J.

1. Introduction

Jupiter's magnetosphere is populated with plasma produced primarily from the ionization of Io's escaping atmosphere. While the specific relative contribution of volcanism and sublimation to Io's atmosphere is an ongoing debate [*Lellouch et al*., 2007, 2015; *Tsang et al*., 2012, 2015], volcanism clearly plays a major role. We would expect, therefore, that the plasma content of Jupiter's magnetosphere might vary with time as Io's volcanic activity changes [*Rathbun and Spencer*, 2010]. An opportunity to explore temporal variability of the Jovian magnetosphere was provided by NASA's Galileo spacecraft which orbited Jupiter for eight years. The Galileo spacecraft was launched on 19 October 1989. After an extensive tour of the inner solar system, getting gravity assists from Venus and Earth (twice), it reached Jupiter on 7 December 1995. After 34 orbits the spacecraft entered Jupiter's atmosphere on 21 September 2003. A brief summary of the Galileo mission is given by *Bagenal et al*. [2004] with details of the mission provided by *Johnson et al*. [1992]; trajectory design described by *D'Amario et al*. [1992] and all of the science instruments are detailed in a special issue of *Space Science Review*, *60*, May 1992. Overviews of the structure of the magnetosphere are provided by *Khurana et al*. [2004] and *Krupp et al*. [2004] as well as by the more recent review of *Bagenal et al*. [2014] in the context of future observations to be made by NASA's Juno mission.

This paper provides a survey of data obtained in the Jovian magnetosphere by the Galileo plasma science (PLS) instrument, led by Louis A. Frank of the University of Iowa. The PLS instrumentation, described by *Frank et al*. [1992], comprises a nested set of four spherical plate electrostatic analyzers and three miniature, magnetic mass spectrometers. Unfortunately, the mass spectrometers proved to be ineffective for routine identification of mass because they provided poor coverage of the sky, and because of low signal-to-noise ratios due to high rates of penetrating radiation. The electrostatic analyzers were designed to measure electrically charged particles (both electrons and positive ions) with energies in the range of ~1 eV to ~50 keV. After orbit insertion the electron sensors suffered degradation and were no longer capable of detecting electrons with energies less than about 100 eV. Because of the sensor degradation, it is not possible to compute plasma parameters for the thermal electrons. For this paper we concentrate on PLS ion data, discussing the measurements in detail in section 2.

Whenever possible, we compare the plasma density determined from the PLS data to values of density derived from the Galileo Plasma Wave Science (PWS) instrument, led by Donald A. Gurnett of the University of Iowa, described by *Gurnett et al*. [1992]. To determine high-resolution (in time and density) plasma density from PWS, electric field measurements require high-rate data that were generally only obtained close to the moons [*Gurnett et al*., 1996, 1998, 2000, 2001; *Kurth et al*., 2001]. Electron densities of poorer temporal density resolution are often available outside of ~25 R_J using the low-frequency cutoff of continuum radiation and inward of ~10 R_J by identifying the upper hybrid resonance frequency, although this is a spectral feature that is not always present.

Previous publications of the Galileo PLS data have concentrated on the flybys of the moons Io [*Frank and Paterson*, 1999a, 1999b, 2000b, 2001b, 2002a], Europa [*Paterson et al*., 1999; *Bagenal et al*., 2015], and the Io plasma torus [*Frank et al*., 1996; *Bagenal et al*., 1997; *Crary et al*., 1998; *Frank and Paterson*, 2000a, 2001a]. Aspects of PLS data obtained in the plasma sheet are discussed by *Vasyliunas et al*. [1997], *Frank et al*. [2002], and *Frank and Paterson* [2002b, 2004]. We compare our results with these previous studies in section 5.

This paper presents a survey of data obtained by the Galileo PLS instrument. This paper is structured as follows: section 2 provides a description of the PLS data set we have selected to analyze; in section 3 we present a brief summary of the analysis techniques employed (more detailed description is provided in Appendix A and the supporting information); section 4 presents the Galileo trajectory and the results of our analysis; section 5 discusses these results, and section 6 presents our conclusions.

2. Galileo Data Set

As originally planned, the Galileo mission would have provided a spectacular amount of data at Jupiter. But because of a major malfunction of the main antenna, the Galileo spacecraft was only able to return a limited amount of data back to Earth. This meant that high-rate data were only obtained on very special events (such as satellite flybys) and much of the data from all of the instruments had to be decimated. A full description of how the PLS data were selected and analyzed is presented in Appendix A and the supporting information. Here we present a summary.

The Galileo PLS instrument (described fully in *Frank et al*. [1992] and *Paterson* [2009]) comprises a set of spherical section electrostatic analyzers with multiple sensors to measure fluxes of particles coming from different directions. Charged particles entering the aperture on the entrance side of the deflection plates are selected according to their directions and their energy per charge. The particles are selected by energy per charge via application of a bias voltage to one of the deflection plates. There are 64 possible (logarithmic) voltage steps covering an energy-per-charge range of ~1 eV to 50 keV. Particles are detected when they enter one of the spiraltron sensors on the exit side of the plates. Each sensor has a different field of view. There are seven sensors arranged to provide near-complete coverage of the sky during the course of spacecraft rotation. The PLS instrument is mounted on a boom on the rotating section of the spacecraft, and the multiple sensors, coupled with spacecraft rotation, provide coverage of approximately 80% of the sky. The instrument is operated in several different preprogrammed modes during the course of the mission. The highest-resolution data are recorded to tape and then transmitted to Earth at the reduced telemetry rate afforded by the low-gain antenna. These high-rate recordings are quite limited in number (usually around satellite encounters) and duration (maximum of 1 h).

The data obtained in each of the 7 sensors over 64 logarithmic energy steps is gathered in four modes with different accumulation times and different methods of decimating the data to accommodate low downlink rates (these processes are described in Appendix A). The three modes used in this paper are as follows: Mode 2, a low-resolution mode with an accumulation time of 0.5 s and where counts are returned for every fourth energy step; Mode 3, a medium-resolution mode with an accumulation time of 0.2667 s and where counts are returned for every third energy step; Mode 4, a high-resolution mode with an accumulation time of 0.15 s and where counts are returned for the majority of energy steps.

Multiple spins of data are collected to form one merged array that is as complete as possible: one merged array may contain data from even anodes with odd anodes in a later (but not necessarily next) spin or may contain data from different spins covering different subsets of energy (see Appendix A and the supporting

information for greater detail of this complexity). Unfortunately, not every actual spin (Galileo spin period ~19 s) returns a data packet, so this process may take anything from ~100 to 130 s for the highest-resolution data to ~200 to 1120 s for the lower modes. During the interval of the merged array we must assume that the plasma environment is stable so that all samples were taken from the same plasma distribution. For this reason we ignore all data from moon encounters (out to 10 R_{Moon}) where the plasma environment likely changes far more quickly than the cadence of our merged arrays.

The net result is a set of energy-time spectra for each of seven anodes in a set of directions per spin of the spacecraft. These can be analyzed in two primary methods: calculation of numerical moments (NM) and by forward modeling (FM).

3. Analysis Techniques

3.1. Numerical Moments

One method of computing parameters and evaluating errors and uncertainties involves a relatively simple summation of fluxes. The parameters derived from the Galileo PLS data by the numerical moments (NM) technique were obtained from the Planetary Data System, and the NM technique is described by *Paterson* [2009]. The PLS measures particle flux as functions of energy per charge and angle (depending on the direction of field of views of the detector at the measurement time). If the plasma is composed of electrons and a single ionic mass/charge species, and the flux is measured with adequate coverage and resolution of both particle energy and direction, then parameters are computed as a summation over velocity of the intensities, with appropriate weighting functions, which include factors of velocity raised to the power 0, 1, 2, etc. This can be done separately for the electrons and for the ions, though we will only discuss ions here. In the case of a single species, particle velocity can be derived directly from the measured energies and directions of the particles. The measured intensities are directly proportional to the phase-space densities of the particles—the particle velocity distribution—and the summations are moments of that distribution. Number density is the zero-order moment. The bulk flow velocity is the first-order moment, pressure the second-order moment, and the temperature can be derived from the pressure and the density.

In the Jupiter system, there are major complicating factors that make this procedure a rough approximation. There are multiple ion species with different mass-to-charge ratio (M/Q) that are only partially separable. While proton ($M/Q = 1$) are easily separated from heavy ions, the known range of heavy ions (O^{++}, S^{+++}, O^{+}, S^{++}, and S^{+}) spans a range of a factor of 4 from $M/Q = 8$ to $M/Q = 32$ which is rarely separated in the Galileo PLS data. Second, particle energies and directions may be poorly covered and/or poorly resolved. This latter complication is especially true for instrument operation during real-time survey (RTS) intervals. The RTS data were transmitted directly to Earth at low bit rates using the low-gain antenna.

To provide approximate heavy-ion parameters, the following procedure is used for computation of numerical moments (NM). First, the heavy ions are treated as a single M/Q species. Because $M/Q = 16$ (amu/e) dominates the ion composition [*Bagenal*, 1994], $M/Q = 16$ is assumed for the numerical moments computation. *Frank and Paterson* [2004] report proton densities based on dayside data from the I33 orbit between ~10 and ~25 R_J at about 10% of the heavy ions, consistent with Voyager measurements [*McNutt et al.*, 1981]. Second, the protons are effectively eliminated by setting a lower cutoff energy per charge which is equal to ¼ the energy per charge of a corotating $M/Q = 16$ ion, which is also ½ the energy per charge for corotating O^{2+}.

The moments are then computed as appropriately weighted summations over energy and direction. The range of errors in parameters derived via the NM technique caused by variation of composition is discussed in detail by *Paterson* [2009]. After the initial computation of the parameters, which include temperature (T), the temperature is used to limit the range of summation to directions and energies that fall within 1 kT of a centroid corresponding to the bulk flow velocity (where k is the Boltzmann constant). The process is iterated once to eliminate samples that may be due to statistical fluctuation of penetrating radiation not being included in the background subtraction, and to mitigate artificially high temperatures due to the presence of trace ions with high M/Q. Full discussion of uncertainties in the plasma parameters derived by this numerical moments technique are discussed in *Paterson* [2009].

Parameters derived by this method have been delivered to NASA's Planetary Data System (PDS) covering all RTS (Real-Time Science) measurements between radial distances of 10–30 R_J. These observations, which span

a combined 129 days, were acquired during 31 of Galileo's 34 orbits at Jupiter. This data set forms the GO-J-PLS-5-RTS-MOMENTS-V1.0 PDS volume and is provided in inertial rotor coordinates, which is a despun spacecraft frame (not in an inertial frame).

3.2. Forward Modeling

A set of energy-time spectra for each of seven anodes over several spin periods (see Appendix A) is fit with a single ion species isotropic Maxwellian distribution in three dimensions. The sensitivity of density to assumptions of composition varies as $(M/Q)^{1/2}$, so our density estimates are not very sensitive to assumptions of the composition. Five free parameters of density, isotropic temperature, and three velocity components are put through a model of the PLS instrument that returns the expected counts given the input parameters, accounting for spacecraft velocity and orientation (anode look direction at all parts of the spin). The mass and charge were separately derived from the *Delamere et al*. [2005] physical chemistry model of the Io plasma torus that is consistent with EUV emissions from the torus observed by the Cassini Ultraviolet Imaging Spectrograph (UVIS) instrument [*Steffl et al*., 2004]. Using the model output, we define a radial profile for mass and charge (M/Q) that is used in our forward model, with ratios ranging from 14 to 27 amu/e (see Appendix A4 and the supporting information for further details). Although early work (based on the propagation of radio waves through the plasma) estimated the abundance of protons in the torus to be 10–15% [e.g., *Tokar et al*., 1982], subsequent work limits this value at only a few percent [*Crary et al*., 1996; *Wang et al*., 1998a, 1998b; *Zarka et al*., 2001]. Outside the torus the proton density derived from Voyager measurements remains ~10% [*McNutt et al*., 1981]. Since the lower energy channels of the GLL PLS data were usually not downloaded, we ignore the contribution of protons in the present analysis of the Galileo PLS data.

The forward model (FM) counts are compared to the observed data (with a background removed) via a reduced chi-square technique, and the free parameters iterated until the minimum reduced chi-square are located.

$$\chi_r^2 = \frac{1}{n-5}\sum_{i=1}^{n} \frac{\left(\mathrm{Obs}_i - \mathrm{Bgnd}_i - \mathrm{Sim}_i\left[n, T, V_r, V_\theta, V_\phi\right]\right)^2}{\sigma_{\mathrm{Obs}_i}^2 + \sigma_{\mathrm{Bgnd}_i}^2}$$

where the merged array has n samples of data, five is the number of free parameters, Obs_i is the total observed counts per accumulation of each sample, Bgnd_i is the background for that data point (identified from the observed data), and Sim_i is the model (see the supporting information for details). The uncertainties in the counts are assumed to be Poisson, such that

$$\sigma_{\mathrm{Obs}_i}^2 + \sigma_{\mathrm{Bgnd}_i}^2 = \begin{cases} \mathrm{Obs}_i + \mathrm{Bgnd}_i & \text{if } \mathrm{Obs}_i - \mathrm{Bgnd}_i > 0 \\ 1 & \text{if } \mathrm{Obs}_i - \mathrm{Bgnd}_i = 0 \end{cases}$$

Uncertainties in the determination of the fitted parameters are found by taking the square root of the diagonals of the covariance matrix for the reduced chi-square fit, where the covariance matrix is the inverse of the curvature matrix [*Wilson*, 2015]. The supporting information describes the method in full detail including prepruning the data to be fitted, limits and constraints used to aid a faster and more physical fit, and postpruning of the fitted data.

In order to carry out a forward model, the observed data must have an identifiable nonzero shape that our Maxwellian function can match. Due to the small geometric factor of PLS and the low density (and therefore low counts) at large distances, there are few data outside 30 R_J that can be fit reliably, so we only analyze data out to 30 R_J.

We explored fitting a sample of the Galileo PLS data with multiple ion species with a specified set of ion ratios (based on the physical chemistry model of *Delamere et al*. [2005]) and found that the temperature of the ions in the multispecies fits were about a factor of 1.4 less than when the spectra were fit with a single ion species (see discussion in Appendix A5). We therefore have divided all ion temperatures by a factor of 1.4.

4. Results

4.1. Data Coverage

The trajectory shown in Figure 1 shows portions of the Galileo trajectory to a radial distance from Jupiter of 30 R_J. In Figure 1 (top row) the crosses indicate the locations of the PLS data used in the forward modeling,

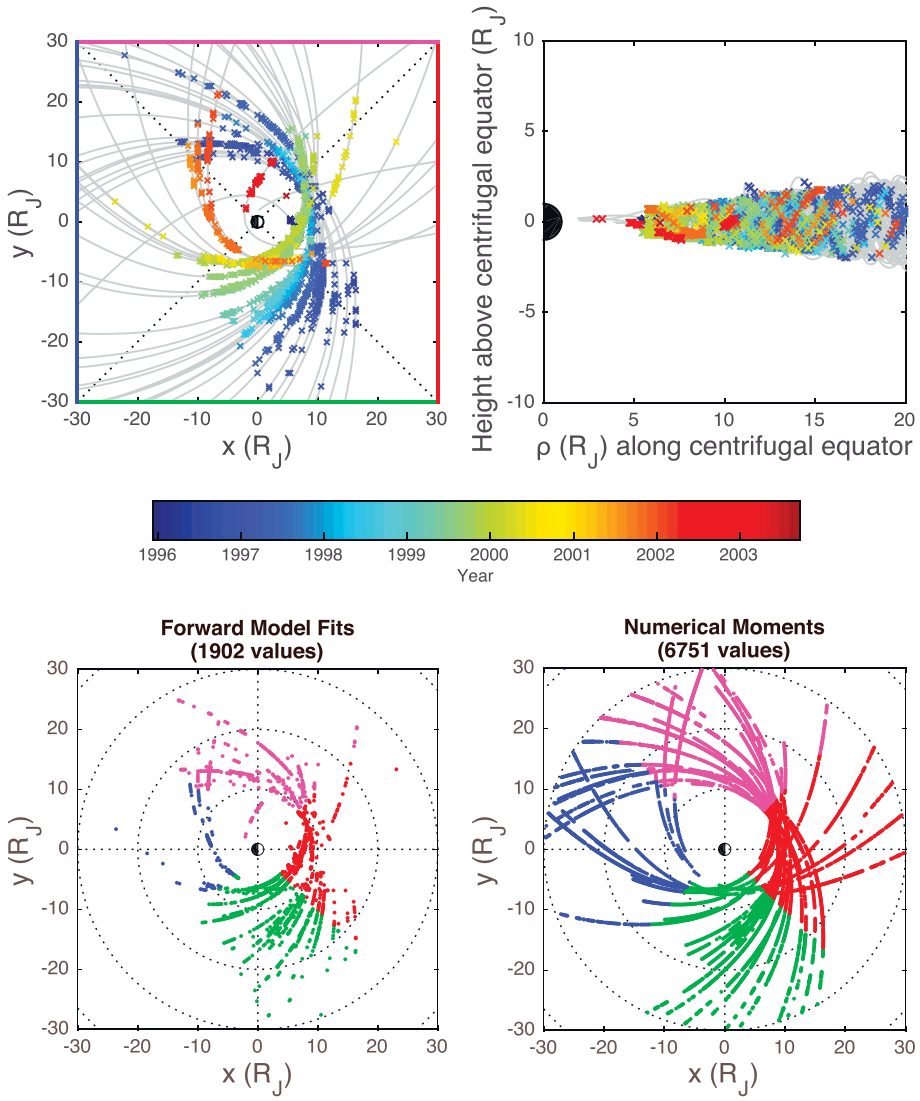

Figure 1. (top row) Galileo trajectory throughout the entire mission shown in grey lines. Times when we are able to fit PLS data are color coded by time. (top left) A top-down view of the spacecraft's path in Jupiter's equatorial plane with Sun to the right. (top right) The coverage with respect to the centrifugal equator. The red, magenta, blue, and green edges show the local time quadrants. (bottom row) Coverage in the equatorial plane (colors corresponding to the local time quadrants) for (bottom left) forward model fits (after pruning) and for (bottom right) numerical moments.

color coded by time throughout the mission. Figure 1 (bottom row) shows how these data are distributed within the four local time quadrants (noon = red, dusk = magenta, midnight = blue, and dawn = green). In Figure 1 (bottom left) we show the locations of the 1902 data points from the forward modeling (after pruning, see Appendix A). Note that there are relatively few points beyond 20 R_J, particularly around noon and midnight. In Figure 1 (bottom right) we show the 6751 data points from the numerical moments technique.

Figure 2 shows the spatial distribution of data that were used in the forward modeling separated by data type or mode. There are very limited times of high-resolution (Mode 2) data, and the largest distribution of data is at the lowest resolution (Mode 2).

4.2. Example Orbit: C23

We have picked C23 as a typical Galileo orbit where we have good coverage of PLS data. This 23rd orbit included a flyby of Callisto and had a perijove distance of 6.55 R_J occurring at 20:00 UTC on 16 September (day of year, DOY, 257) 1999. Figure 3 shows plasma parameters derived from PLS data using forward

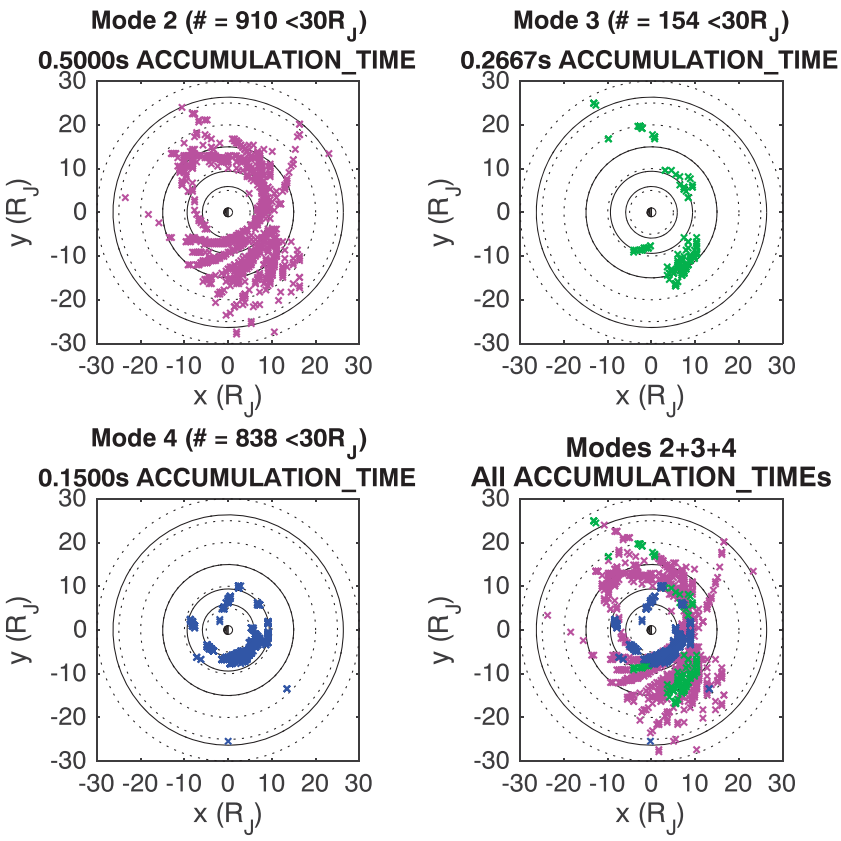

Figure 2. Spatial distribution (projected onto the jovigraphic equator) of data used in forward modeling (after pruning) for low, medium, and high accumulation times (Modes 2–4).

modeling. The colors represent the local time of the data point. The three components of plasma flow velocity are shown in spherical coordinates (r, θ, ϕ) in the jovigraphic system after accounting for the spacecraft velocity. The jovigraphic coordinate system has z aligned with Jupiter's spin axis; x is in the plane that contains the direction of the Sun and the spin axis. The spherical version of the system (r, θ, ϕ) has r as radial distance, and θ is the angle from the equatorial plane and is the azimuthal direction (for description of Jovian coordinate systems see http://lasp.colorado.edu/home/mop/missions/juno/coordinates/).

Figure 4 shows a comparison of plasma parameters derived by the numerical moments (NM) and forward modeling (FM) techniques. For the numerical moments technique the magnitude of the flow is given in the despun spacecraft frame. Note that the Galileo spacecraft passed counterclockwise around Jupiter so that around closest approach the spacecraft velocity is approximately azimuthal with a maximum value of about 25 km/s, less than the uncertainty in the flow determination. The numerical moments flow magnitude is compared with the dominant flow component, V_ϕ, from the forward modeling. The two techniques show similar values with comparable levels of uncertainty in the determination of the parameters.

In Figure 5 we have replotted the parameters from the forward modeling technique to the C23 orbit as a function of radial distance, color coded for local time quadrant (as in Figure 1). The azimuthal component of the flow, V_ϕ, is between 60 and 100% of corotation. In the noon quadrant (red) the nonazimuthal components (~20 km/s) are radially inward and northward. As we show below, this local time flow behavior is not persistent through the mission and seems to be specific to the C23 orbit. The decreasing density and increasing temperature with distance from Jupiter are persistent profiles that are seen throughout the Galileo mission, as discussed further in sections 4.5 and 4.6.

4.3. Example Orbit: I27

An alternative method of deriving the local plasma density is to look at radio emissions that exhibit a frequency cutoff at the local upperhybrid frequency (f_{uh}). The observations presented herein are from the

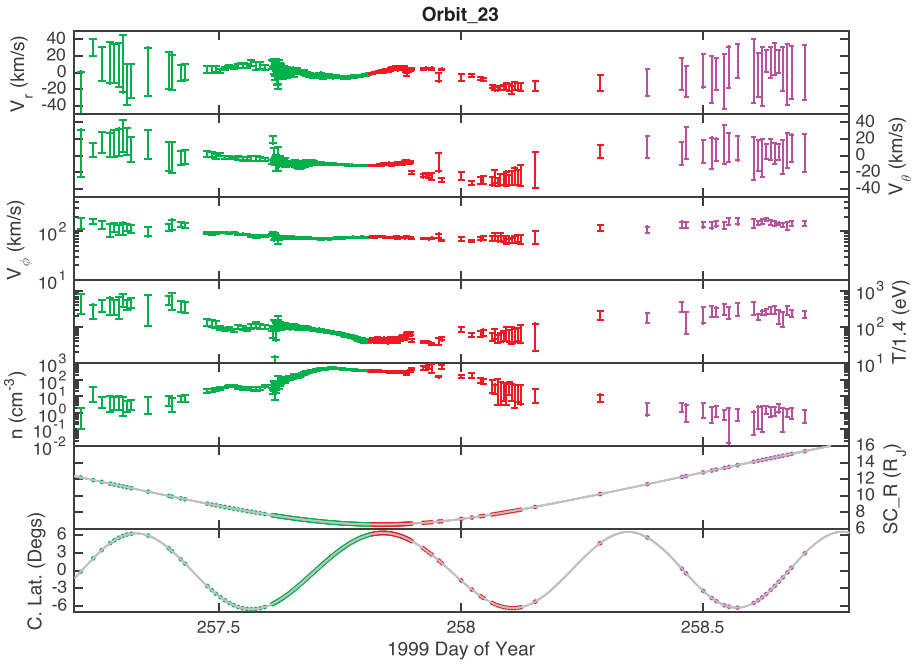

Figure 3. Plasma parameters from forward modeling of PLS data from orbit 23 over 1999 DOY 257 and 258. Top five plots are, respectively, the three components of flow velocity (planet-centered spherical coordinates), the temperature, and the ion density. The bottom two plots show the radial distance and centrifugal latitude. The colors represent the local time (LT) of the data point: green = dawn (LT = 0300–0900), red = noon (LT = 0900–1500), purple = dusk (LT = 1500–2100), and blue = midnight (LT = 2100–0300), as in Figure 1.

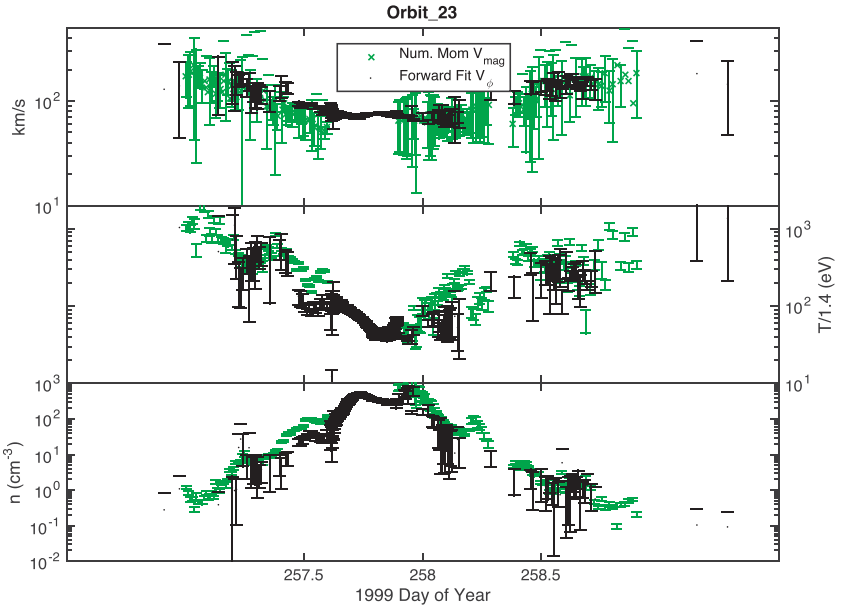

Figure 4. Comparison of parameters (flow, ion temperature, and ion density) derived from PLS data via numerical moments (green) and forward modeling (black) for orbit C23, over 1999 DOY 257 and 258. For the forward fits the flow speed is the azimuthal component (in planet-centered spherical coordinates), while for the numerical moments the magnitude of the flow in the spacecraft frame is shown.

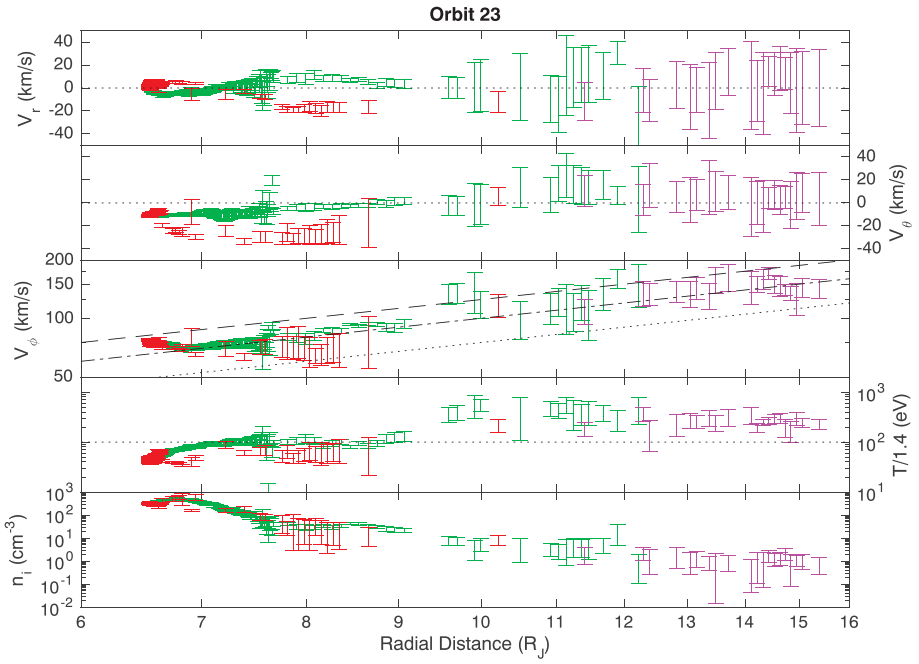

Figure 5. Forward modeled plasma parameters versus radial distance in orbit 23. The parameters shown are, from top to bottom, the azimuthal component of flow velocity, the ion temperature, and the local ion density. The dashed lines in the azimuthal flow plot represent the radial profiles of 100%, 80%, and 60% rigid corotation. The dashed line in the temperature plot is a fiducial mark at the typical value of 100 eV. Green = dawn (LT = 0300–0900), red = noon (LT = 0900–1500), purple = dusk (LT = 1500–2100), blue = midnight (LT = 2100–0300).

Galileo plasma wave instrument that is described thoroughly in *Gurnett et al.* [1992]. The instrument measures the electric field component of waves in the frequency range of 5.62 Hz–5.6 MHz using a single-axis dipole antenna with an effective length of 6.6 m and magnetic fields in the frequency range of 5.62 Hz–160 kHz with a pair of magnetic search coils. The high-frequency search coil is used for frequencies above 2.4 kHz. The low-frequency search coil is tuned for frequencies below 2.4 kHz. A failure in the low-frequency search coil or its signal path on 14 September 1997 during the tenth orbit resulted in increased levels of noise and a serious reduction in sensitivity for frequencies below 2.4 kHz. Hence, low-frequency magnetic field measurements for the E11 flyby and later are not very useful. However, in some cases, intense electromagnetic signals can be seen, and this is sufficient to justify the identification of some waves as being electromagnetic as opposed to electrostatic. The lack of magnetic signatures in this frequency range, however, does not justify the identification of electrostatic modes. The primary measurements are made using a multichannel analyzer, a medium frequency receiver, and a high-frequency receiver to provide a single 152-channel spectrum over the entire frequency range once every 18.67 s. Using local measurements of magnetic field allows one to then determine the local plasma frequency, and hence local electron density.

Figure 6 shows a comparison of plasma conditions from the Galileo PWS and PLS instruments. At Figure 6 (top) we show a frequency-time spectrograph of PWS electric field data for the I27 orbit. The 24 h of data were obtained on DOY 53 2000 when the spacecraft traversed in from 11.1 R_J in past Io and out to 10.5 R_J. Rising and then falling across the plot is a line of emission corresponding to the upper hybrid frequency of the plasma. Superposed on the spectral plot is a line for the upper hybrid frequency derived from the density determined from PLS numerical moments. The PLS value for the upper hybrid frequency (based on the PLS numerical moments electron density estimates) tracks the PWS lower frequency cutoff quite well, falling below the PWS emission line by less than a factor of 2 for most of the region. In Figure 6 (middle) we show values of local electron density derived from PLS data on orbit 27 that derived from both the numerical moments and forward modeling techniques. The PLS electron density is calculated from the ion data assuming the ion charge state ($Q = 1$ for the NM technique and for the FM values Q is from the profile shown in Figure A4) and that the plasma is charge neutral. The region close to Io is excluded where the data are

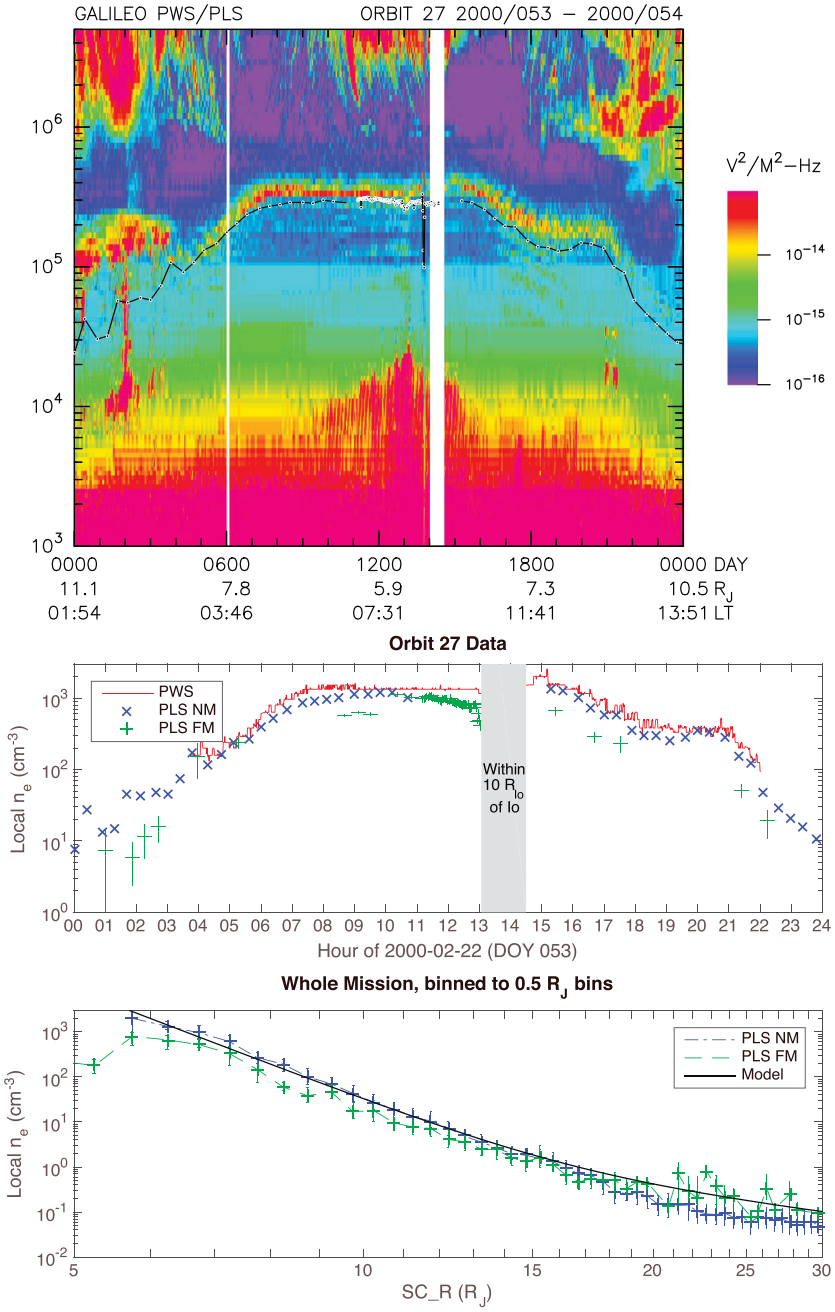

Figure 6. Density comparisons for orbit 27 on 2000 DOY 053. (top) Frequency-time spectrogram of electric field measured by the Galileo PWS instrument. Overplotted in black is the upper hybrid frequency derived from the electron density derived from the numerical moment (NM) analysis of the PLS data. (middle) Electron density profiles over orbit 27 derived from the upper hybrid emission line in the PWS data as well as derived from NM and forward model (FM) analyses of the PLS ion data (multiplying the total ion density by assumed average charge state). (bottom) Electron density profiles over the whole Galileo mission derived from PLS data via NM and FM analysis techniques, plus the empirical radial profile from *Bagenal and Delamere* [2011].

complicated by rapid changes in plasma conditions due to the interaction with the moon's atmosphere [*Gurnett et al.*, 2001; *Frank and Paterson*, 2001b; *Dols et al.*, 2012].

Figure 6 (bottom) shows radial profiles of local electron density derived from all available PLS data from the whole Galileo mission from numerical moments and forward modeling multiplied by the assumed charge state of the ions. All data are binned in 0.5 R_J bins with the median and 25th and 75th percentile values

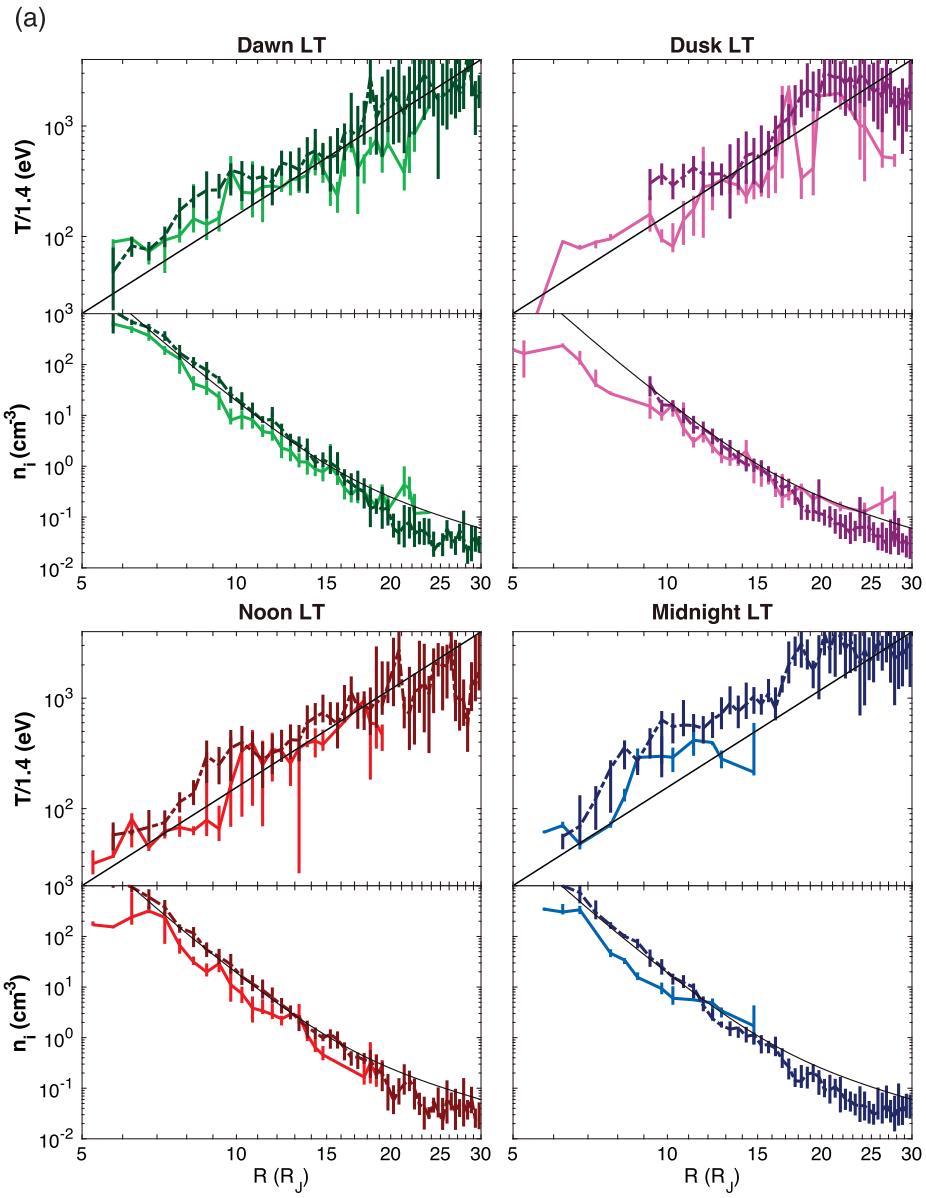

Figure 7. (a) Ion temperature and ion density from the whole mission in 0.5 R_J bins and sorted by local time (LT). The colors represent the local time (LT) of the data point: green = dawn (LT = 0300–0900), red = noon (LT = 0900–1500), magenta = dusk (LT = 1500–2100), and blue = midnight (LT = 2100–0300). PLS data are analyzed using the numerical moments (dark colors, dashed line) and forward modeling (light colors, solid line). The black curves show a fiducial line for temperature and the empirical density profile from *Bagenal and Delamere* [2011] divided by average charge state to give ion density. (b) Plasma flows from the whole mission in 0.5 R_J bins and sorted by local time (LT). The color scheme is the same as Figure 7a. PLS data are analyzed using the numerical moments (dark colors, dashed line) to derive magnitude of the flow in spacecraft coordinates and forward modeling (light colors, solid line) for three components of flow in planet-centered spherical coordinates. The dashed black lines show 100%, 80% and 60% of corotation. (c) Binned information from forward modeling versus local time (LT) with Sun to left. A: number of points in each bin. B: sum of ion densities. C: ion temperature. D: azimuthal flow. The radial bins are logarithmic between 5 and 30 R_J.

plotted. For reference we have included the radial electron density profile derived from an empirical fit to a combination of earlier data sets by *Bagenal and Delamere* [2011] where density (in cm^{-3}) at distance R (in R_J) is given by

$$N(r) = 1987(R/6)^{-8.2} + 14(R/6)^{-3.2} + 0.05\,(R/6)^{-0.65}\,(\mathrm{cm}^{-3})$$

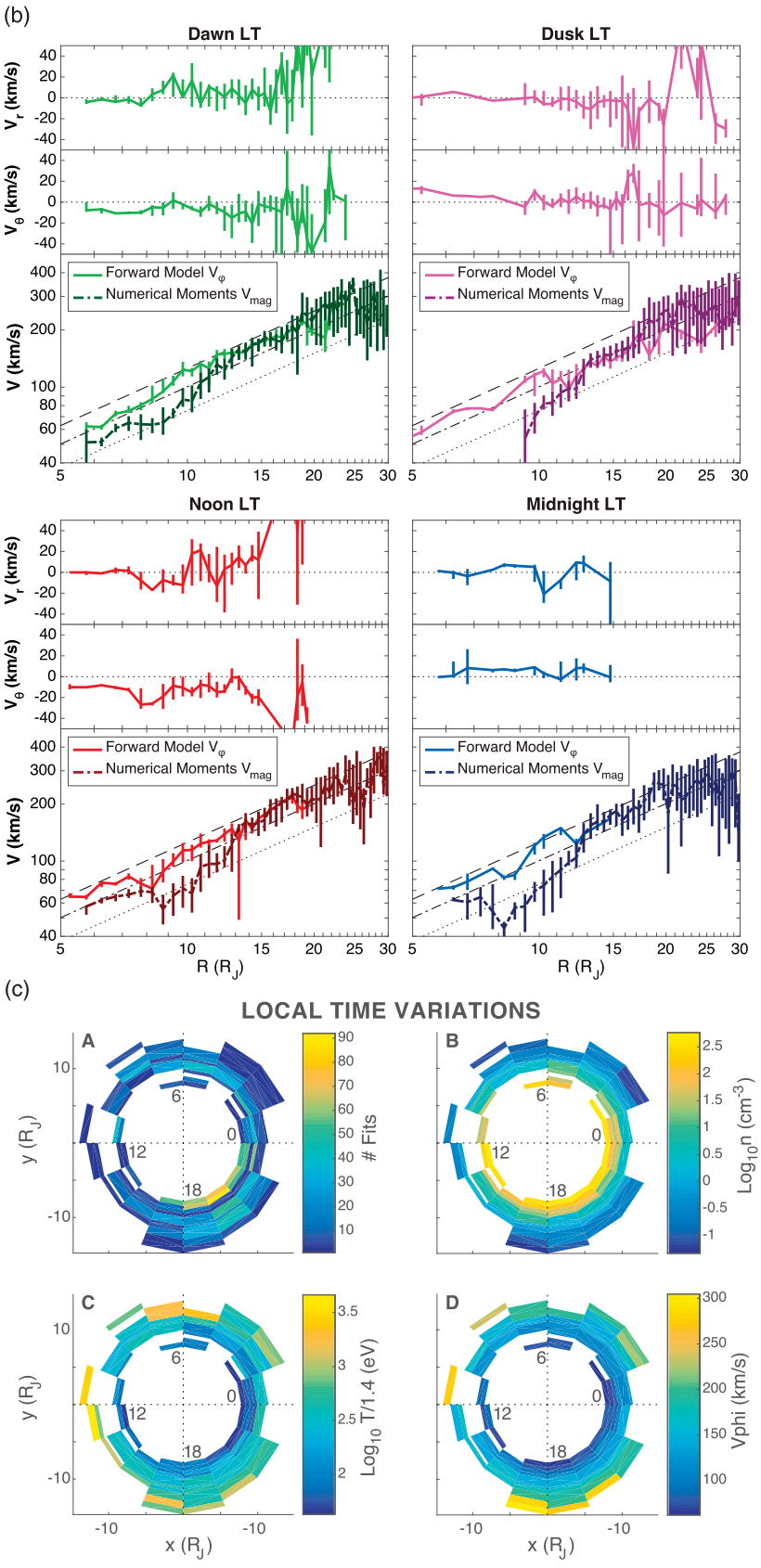

Figure 7. (continued)

This profile is based on Voyager PLS and PWS data sets plus early PLS numerical moments [*McNutt et al*., 1981; *Bagenal and Sullivan*, 1981; *Frank et al*., 2002; *Barnhart et al*., 2009]. Recall that the PLS densities derived via the numerical moments method assume a constant composition ($M/Q = 16$ and O^+), while the forward fitting used a variable composition with distance (see Appendix A). We have multiplied the local ion densities from both analyses of the PLS data by a profile of average charge state based on UV emissions and physical chemistry models in the torus out to 8 R_J (see Appendix A). The Galileo PLS profiles show remarkable consistency (at least to a factor of 2) with the *Bagenal and Delamere* [2011] profile between 6 and 30 R_J while the density drops by nearly 5 orders of magnitude.

4.4. Variation With Local Time

To investigate a systematic variation with local time, we present in Figures 7a and 7b four panels with parameters derived from the two techniques for analyzing the PLS data binned in radial steps of 0.5 R_J (when there are at least three points per bin) and in local time (LT) quadrants for dawn (0300–0900 h LT), noon (0900–1500 h LT), dusk (1500–2100 h LT), and midnight (2100–0300 h LT). Median values are plotted for each bin with error bars corresponding to 25th and 75th percentiles. In Figure 7a we show the local time comparison of local ion density and of ion temperature (that has been divided by 1.4 to compensate for using a single species to fit spectra that we know comprise multiple ion species). The empirical profile of electron density from *Bagenal and Delamere* [2011] has been divided by the charge density profile (Appendix A) to provide a reference ion density. For a fiducial curve for the temperature profiles we have drawn a diagonal line across the plots.

Figure 7b shows binned values of V_r, V_θ, and V_ϕ from the forward modeling to PLS data for the four local time quadrants. The radial profiles of V_r, V_θ are very noisy and do not show a consistent pattern. The azimuthal flow V_ϕ is compared with the magnitude of flow derived from the numerical moments technique and fiducial lines for 60%, 80%, and 100% of corotation with Jupiter. The V_ϕ from forward modeling shows persistent values between 80% and 100% of corotation for all local time quadrants out to ~15 R_J. Beyond 15 R_J there is limited coverage of data that can be analyzed with the forward modeling technique except in the dusk quadrant where (between 20 and 30 R_J) the azimuthal flow slows closer to 60% of corotation or about 200 km/s, consistent with Voyager plasma data [*McNutt et al*., 1981]. The numerical moments show slower flow speeds V_{mag} than the forward fit values of V_ϕ closer in and faster flow speeds farther out. This difference is only partially explained by the constant $M/Q = 16$ value used for the numerical moments compared with the variable M/Q profile for the forward modeling. We also note that the flow speed V_{mag} plotted for numerical moments is calculated in the spacecraft frame. The spacecraft speed can become significant in the torus (25 km/s), but this does not explain why the greatest deviation from corotation is around 9 R_J (rather than closest approach to Jupiter) and is inconsistent with the azimuthal speeds derived from the forward modeling technique. We do not have an explanation for this difference.

To further explore the possibility of local time variations, we plotted the FM parameters binned logarithmically in radial distance (5 to 30 R_J) and 16 local time bins in Figure 7c. While the distribution is sparse (the top left plot shows the number of points in each bin), there does not seem to be a consistent pattern in local time for plasma density, temperature, or azimuthal speed.

4.5. Variation With Longitude

In Figure 8 we have repeated a similar radial binning as in Figure 7 except the quadrant bins are in longitude, the system that corotates with the planet. The traditional System III Longitude is west longitude (WLon) that increases for a stationary observer with time (and forms a left-handed coordinate system). East longitude (ELon) is defined to form a right-handed system, decreases with time, and is computed as 360° WLon. Figure 8 shows four quadrants organized to compare equator crossings where $22° < \text{ELon} < 112°$ and $202° < \text{ELon} < 292°$ (or $248° < \text{WLon} < 338°$ and $68° < \text{WLon} < 158°$) and when the spacecraft is above the centrifugal equator ($112° < \text{ELon} < 202°$ or $158° < \text{WLon} < 248°$) or below the centrifugal equator ($292° < \text{ELon} < 22°$ or $338 < \text{WLon} < 68°$). In Figure 8a we have plotted ion density and temperature, while Figure 8 b shows plasma flow. In Figure 8a we added values of ion temperature obtained 6–9 May 1997 during the Galileo G8 orbit and reported by *Frank and Paterson* [2002b]. They report values of particularly high ion temperatures (few keV), derived via the numerical moments technique, for the longitude range of 267° <

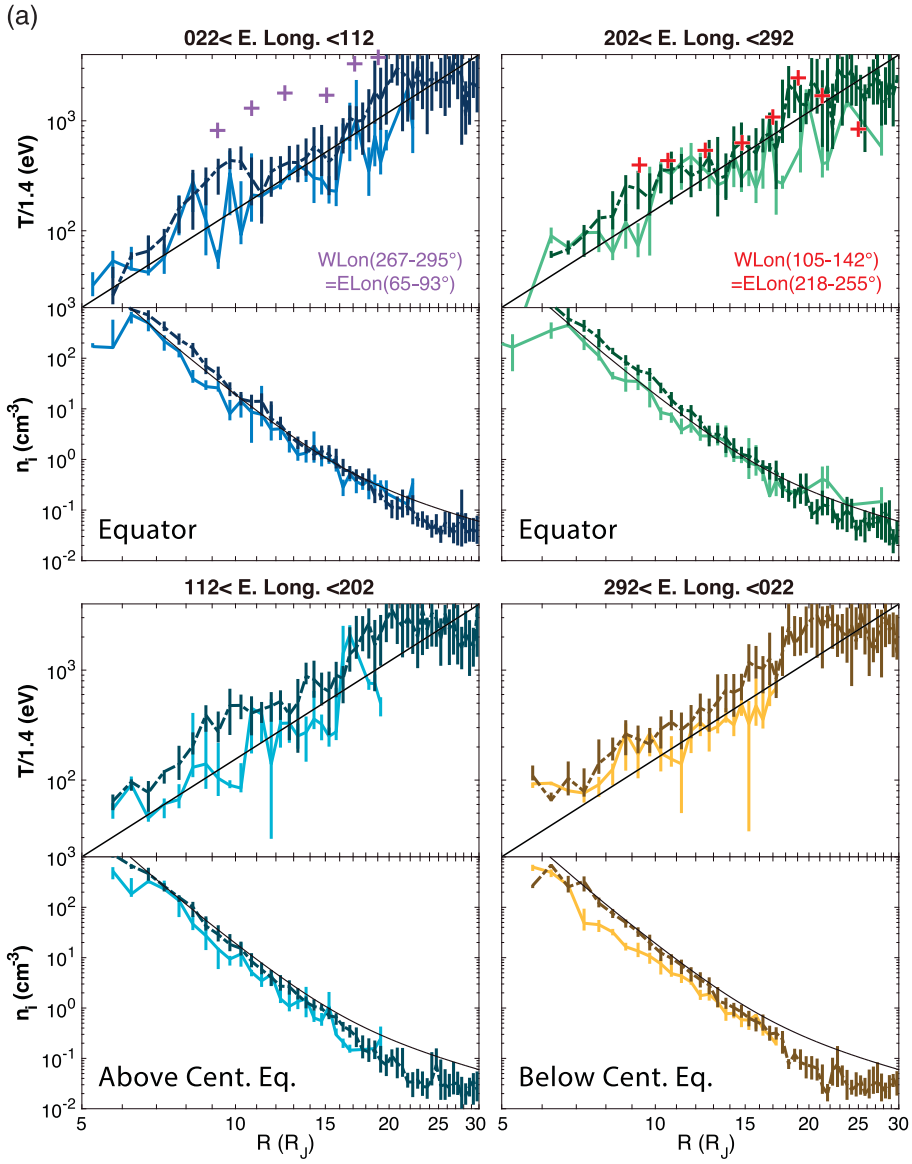

Figure 8. (a) Same as 7a except binned in longitude quadrants. The top panels are for longitudes close to the centrifugal equator. The bottom left and right plots show data where the spacecraft was above and below the centrifugal equator, respectively. Crosses show points from [*Frank and Paterson*, 2002a]: red for WLon (105–142°) = ELon(218–255); purple for WLon(267–295°) = ELon(65–93°). (b) Same as 7b except binned in longitude quadrants. (c) Binned information from forward modeling versus east longitude (ELon). A: number of points in each bin. B: sum of ion densities. C: ion temperature. D: azimuthal flow. The radial bins are logarithmic between 5 and 30 R_J. East longitudes where the jovigraphic, magnetic, and centrifugal equators cross are 68° and 248°. The spacecraft was at a maximum distance above (below) the centrifugal and magnetic equators at ELon = 158° (338°).

WLon < 295° (65° < ELon < 93°) when the spacecraft is near the centrifugal equator. On the opposite side of Jupiter they report temperatures similar to those derived in this study.

Using the fiducial curves to guide the eye, it is hard to see a persistent pattern with longitude in these plots. So we binned the three main plasma properties derived via forward fitting—density, temperature, and azimuthal flow—in radial distance and longitude in Figure 8c. The top left plot shows that the distribution of points from the FM fits is more uniform in longitude than in local time. While density and V_ϕ look very uniform with longitude, there seems to be lower ion temperatures between ELon = 90–180° (WLon = 180–279°) for the

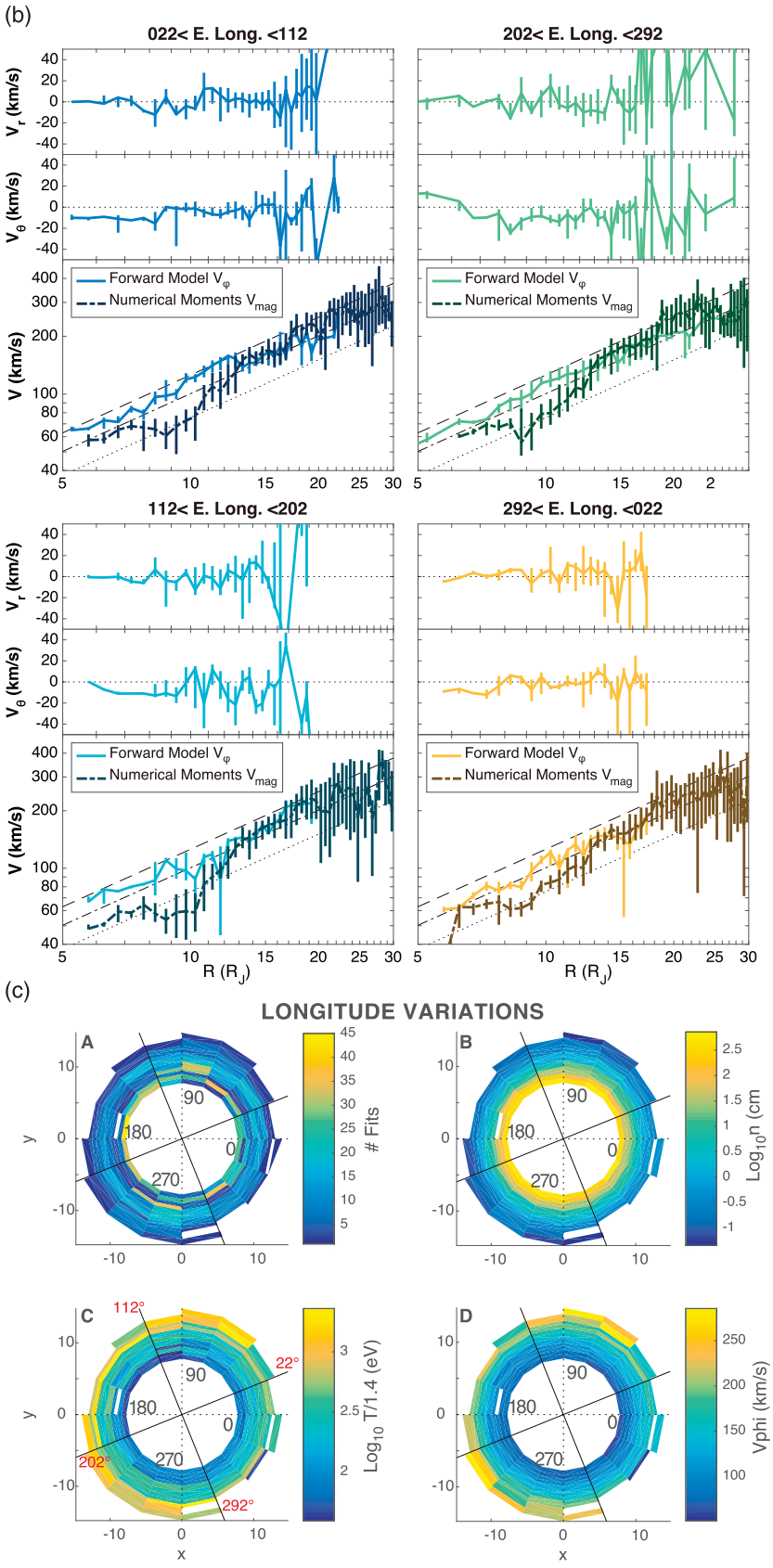

Figure 8. (continued)

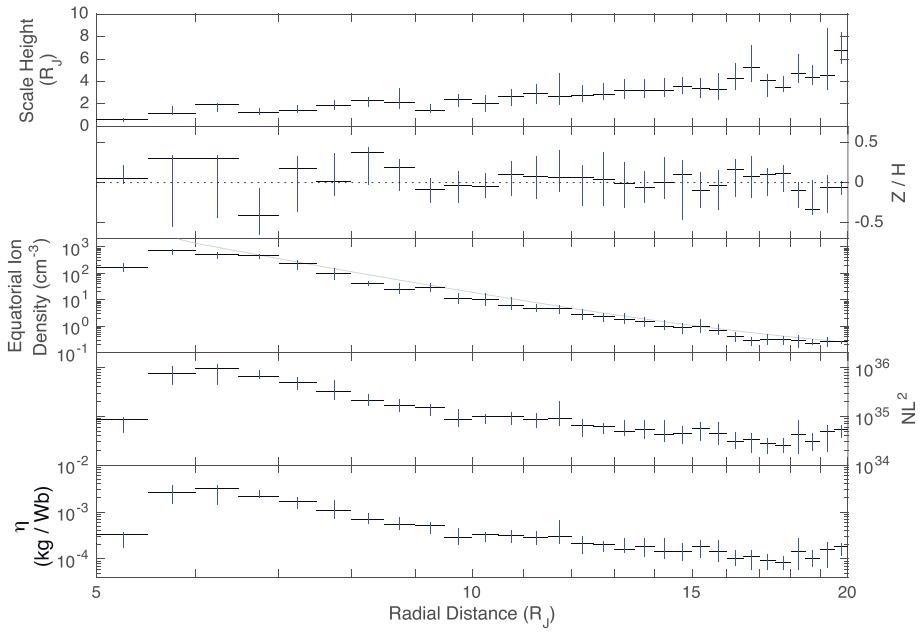

Figure 9. Radial profiles of (i) scale height (H) for distribution of plasma along the magnetic field; (ii) ratio of spacecraft distance from the centrifugal equator (*z*) to scale height (*H*); (iii) equatorial density, compared to the empirical model profile (grey) from *Bagenal and Delamere* [2011]; (iv) flux tube content; and (v) integrated mass per unit of magnetic flux. Quantities have been calculated from plasma parameters derived via forward modeling and averaged in 0.5 R_J bins with the median values plotted with errors representing the 25th and 75th percentiles in each bin.

innermost couple of radial bins (5–7 R_J). Farther out the longitudinal variation does not seem to persist. We return to this topic for further discussion in section 5.

4.6. Flux Tube Quantities

To relate locally measured quantities to bulk properties of the plasma sheet, we need to consider the distribution of plasma along the magnetic field. In the rotation-dominated magnetosphere of Jupiter the plasma is confined to the centrifugal equator that is located two thirds of the way from the rotation equator toward the magnetic equator. In the case of the tilted dipole approximation for the magnetic field of Jupiter, this means a tilt of $2/3 \times 9.5° = 6.3°$. For a single ion species the density at centrifugal latitude θ_c and vertical distance from the centrifugal equator $z = R \sin(\theta_c)$ along the field can be described by a Gaussian function [*Hill and Michel*, 1976]

$$N(z) = N(z=0)\,\mathrm{exp}{-}(z/H)^2$$

where the scale height is

$$H = \left[2/3\ \mathrm{kT/m}\Omega^2\right]^{1/2} = 0.64 R_J \left[V_{co}/V_\psi\right]^2 \left[T_i(\mathrm{eV})/A_i(\mathrm{amu})\right]^{1/2}$$

Thus, to convert from local density at the spacecraft location, *z*, off the centrifugal equator, to the equatorial density, we need to multiply the local density by exp $(z/H)^2$. For a discussion of the distribution along the field for a multispecies plasma see *Bagenal* [1994], but, given the limitations of the data studied here, we argue that a single species approximation is reasonable.

Figure 9 shows that for the observed ion temperatures (derived via forward modeling) the scale height *H* increases with radial distance from about 1.5 R_J in the torus to 4 R_J in the plasma sheet at 20 R_J. The Galileo spacecraft did not venture far from the jovigraphic plane so that the distance from the centrifugal equator, *z*, remained within half a scale height, so the calculated equatorial density is not very different from locally measured density. Figure 9 shows that the equatorial radial ion density profile averaged over the whole Galileo mission is pretty close to the empirical profile derived earlier from Voyager and Galileo data by

Bagenal and Delamere [2011] (shown divided by assumed charge state of ions at each radial distance to convert electron to ion density).

For calculations of rates of radial transport (by centrifugally driven flux tube interchange [*Hill*, 1976]) we need to calculate the total amount of ions in a flux shell. Specifically, we need (assuming a dipole field)

$$NL^2 = 4 \times 10^{30}\, L^3\, n_i(z=0)H$$

Alternatively, one can use the mass of ions along the flux tube per unit magnetic flux

$$\eta\,\mathrm{kg/Wb} = 2\, m_i n_i(z=0)\mathrm{H/B}(z=0)$$
$$= 1.2\times 10^{-7} n_i(\mathrm{cm}^{-3}) H(R_J)\, A_i(\mathrm{amu})[R(R_J)/6]^3$$

These two flux tube quantities are plotted at the bottom of Figure 9. They are consistent with previous estimates derived from Voyager data [*Bagenal and Sullivan*, 1981; *Bagenal*, 1994] but approximately two thirds of values derived by *Crary et al*. [1998] from Galileo's first traversal of the torus and the profile derived from Cassini UV emissions by *Delamere et al*. [2005].

5. Discussion

Overall, we find systematic variations in density and temperature in with radial distance. Density drops by 5 orders of magnitude, and ion temperature increases by a factor ~40 between 6 and 30 R_J. The flow is largely azimuthal between 80 and 100% of corotation with Jupiter. We find no persistent variations of V_ϕ with local time except for a suggestion that the dusk flows are closer to 60% of corotation between 20 and 30 R_J. Note that if there were persistent local time variations in azimuthal speed, one would expect to see a corresponding anticorrelation with density—the density (and magnetic field magnitude) increasing when the azimuthal flow slows down.

The lack of persistent variation in azimuthal flow with local time in the Galileo PLS data out to 30 R_J is in contrast to the significant dawn-dusk asymmetry in V_ϕ derived from particle anisotropies measured by the Galileo Energetic Particle Detector (EPD) instrument and reported by *Krupp et al*. [2001a, 2001b] and *Woch et al*. [2002]. The EPD anisotropy data suggest flows in the outer magnetosphere on the dawnside several times faster than on the duskside. At distances of only 30 R_J they suggest a factor of 2 difference with the dawnside flows a factor of 2 higher than those on the dusk side of the magnetosphere. These conflicting results have been discussed at scientific meetings over the past dozen years, but a resolution remains unclear.

The values of V_r and V_θ derived from the forward modeling vary around zero with increasing scatter farther out. Using their empirical radial density profile, *Bagenal and Delamere* [2011] derive radial outflow speeds reaching 12 to 80 km/s at 30 R_J for iogenic plasma production rates 0.26 and 1.4 t/s. Unfortunately, the quality of the data is not able to provide an accurate assessment of such flows beyond about 15 R_J. Again, there does not seem to be a systematic local time effect.

The apparent lack of variation with System III Longitude comes after decades of observations and discussions of System III variations in the Io plasma torus, as reviewed by *Thomas et al*. [2004] and *Steffl et al*. [2006]. From ground-based observations System III Longitude variations in optical S^+ emissions were observed. Since these optical emissions are sensitive to density, it was concluded that it must be the density that is varying with longitude. *Herbert et al*. [2008] shows several ground-based observations of the "ribbon" region at ~6 R_J that exhibit longitudinal variations in vertical extent of the torus emissions, presumed to be related to the ion temperature parallel to the magnetic field. They show variations of ion temperature with longitude that change considerably (greater than a factor of 3) from observation to observation, with temperature minima that range between WLon ~ 120 and 300°. Ultraviolet emissions from the dense, hot outer torus were observed to show System III variations. These UV emissions are most sensitive to electron temperature, as we discuss further below.

Galileo traversals of the plasma sheet also showed occasions where the ions seemed to be consistently hotter in the plasma sheet (9–30 R_J) on one side of Jupiter than the other, as reported by *Frank and Paterson* [2001a, 2002b, 2004] and *Frank et al.* [2002]. For example, we show the temperatures derived by *Frank and Paterson* [2002b] from PLS data obtained on 6–9 May 1997 on the G8 orbit in Figure 8a.

We have looked at the numerical moments for each Galileo orbit [*Paterson*, 2009] and find that there are indeed times when there seem to be noticeable longitude variations in ion temperature (perhaps anticorrelated with density), specifically on orbits G7, G8, G9 (in the first half of 1997), orbits E26, G29 (in 2000), and orbit I32 (October 2001). But the System III Longitude variation in ion temperature is not discernable in PLS numerical moments from other orbits nor clear from the profiles of Ti derived from numerical moments for different longitude quadrants shown in Figure 8a.

When we examine the ion temperatures derived via forward modeling (Figure 8a), we see that the profiles perhaps tend to be slightly lower than the profiles derived via numerical moments, but there does not seem to be a persistent longitudinal variation. To dig deeper into the issue of longitudinal variability, Figure 8c shows the plasma parameters binned in radial distance (logarithmically between 5 and 30 R_J) and longitude over the whole Galileo mission. The only significant variation in ion temperature is limited to radial distances of 5–7 R_J and with a decrease in temperature (30–50 eV) at 90° < ELon < 180° (180° < WLon < 270°). On the opposite side of Jupiter at this distance the average temperatures are greater than 100 eV. This longitudinal region of lower ion temperatures is similar to the region of lower (parallel) ion temperatures reported by *Herbert et al*. [2008] from ground-based observations of the torus ribbon (WLon ~ 120–300°). But within this same longitudinal range lies the region (WLon = 267–295°) where *Frank and Paterson* [2002b] report higher temperatures between 9 and 30 R_J for the G8 orbit, suggesting that longitudinal asymmetries vary with distance or time.

Such a possibility of intermittent variation in plasma properties is consistent with the findings of *Steffl et al*. [2006] who analyzed several months of UVIS observations of the torus taken when Cassini flew past Jupiter in late 2000 to early 2001. The S^+ mixing ratio and electron density show an ~ ±20% longitudinal variation approximately in phase with each other. The mixing ratio of S^{+++} and the electron temperature show similar variations, also approximately in phase with each other, but are approximately 180° out of phase with the variation of S^+ and electron density. The mixing ratio of the dominant ion S^{++} and O^+ shows a much smaller (few percent) longitudinal modulation. The ~50 days of continuous observations revealed a systematic variation in the amplitude of these modulations over ~30 days. *Steffl et al*. [2008] was able to match the System III Longitude modulation by applying the *Delamere and Bagenal* [2003] physical chemistry model for the torus with an imposed variation in a small (~0.2%) fraction of superthermal (~50 eV) electrons centered around WLon = 290° (ELon = 70°). This is roughly similar to the region (WLon ~ 120–300°) of hotter ion temperatures derived from ground-based observations by *Herbert et al*. [2008].

Imposing a second subcorotating hot electron variation produces a beat frequency modulation, matching the ~30 day change in the amplitude of the System III variation. *Hess et al*. [2011] argue that the System III variation of hot electrons is consistent with the current system that couples the torus to the ionosphere of Jupiter being modulated by the detailed structure of the magnetic field close to the planet. They propose that the subcorotating hot electrons are produced when empty flux tubes move inward, as observed by *Kivelson et al*. [1997] and *Thorne et al*. [1997], during the flux tube interchange process that is responsible for radial transport.

The net conclusion of the *Steffl et al*. [2006, 2008] modeling of the UVIS data is that several properties of the torus plasma (electron density and ion composition) can exhibit System III Longitude variations and that these variations come and go on longer timescales of several weeks. The UV emissions of the torus do not reveal any information about ion temperature, but the physical chemistry models show that ion temperature depends on plasma production and radial transport rates [*Delamere and Bagenal*, 2003; *Delamere et al*., 2004, 2005]. It seems feasible, therefore, that the intermittent longitude variations in ion temperature observed in the Galileo PLS data could be generated in a similar way to the torus UV modulations. Such a possibility could be tested with the physical chemistry model as well as through further observations of the torus by the Extreme Ultraviolet Spectroscope for Exospheric Dynamics (EXCEED) UV telescope on the Japan Aerospace Exploration Agency (JAXA) Hisaki spacecraft in Earth orbit [*Yoshioka et al*., 2013; *Yoshikawa et al*., 2014] and in situ measurements of the plasma sheet by NASA's Juno spacecraft.

6. Conclusions

Analysis of the PLS data via the numerical moments technique (over 6700 points) and forward modeling (nearly 2000 points) provides an extensive survey of plasma parameters (density, temperature, and flow) in

the plasma sheet between 5 and 30 R_J. The two techniques are in pretty good agreement with each other, and the densities from PLS agree (especially in the high-density regions of the torus) to within a factor of 2 with values derived from PWS measurements. A list of major conclusions from this survey of Jupiter's plasma sheet is as follows:

1. The density of plasma near the centrifugal equatorial plane drops from electron density values of about 2000 cm^{-2} in the Io plasma torus at 6 R_J to values of about 0.05 cm^{-2} at 30 R_J, with no persistent systematic variations with longitude or local time. This radial profile of density is consistent with the empirical profile derived primarily from Voyager data by *Bagenal and Delamere* [2011]. We conclude that while Io's volcanoes have been active over the Galileo epoch [*Rathbun and Spencer*, 2010], the plasma production and transport has remained constant to about a factor of 2.
2. Contrary to the concept of adiabatic cooling on expansion, the plasma in Jupiter's plasma sheet heats up as it expands out from Io's orbit (where Ti ~ 60–80 eV) at ~6 R_J to a few keV at 30 R_J. There is no long-term, systematic variation in ion temperature with local time.
3. The only persistent variation in ion temperature with longitude is the presence of colder temperatures in the inner region (5–7 R_J) in the longitude range of WLon = 180–279°. This latter finding is different from the findings of *Frank and Paterson* [2001a, 2002b, 2004] and *Frank et al*. [2002] who found higher temperatures in a similar longitude region (WLon = 267–295°). Further examination of ion temperatures from all Galileo orbits suggests that System III variations in ion temperature are transitory on timescales of weeks.
4. The plasma flow derived via forward modeling is dominated by azimuthal flow that is between 80% and 100% of corotation out to 20 R_J. The numerical moments technique indicates a significant deviation from corotation around 9 R_J. We have no explanation for this difference. Azimuthal flows from both techniques seem to be slightly more corotational on the dawnside than at dusk. This is in the same direction as the dawn-dusk asymmetry reported by *Krupp et al*. [2001a, 2001b] and *Woch et al*. [2002] but much weaker than the factor of 2 they derive from Galileo EPD data.
5. Vertical and radial flows are small and variable between 5 and 30 R_J. They are poorly determined beyond about 15 R_J. There is no clear, persistent variation of these flow components with either local time or longitude.
6. Calculations of flux tube content are consistent with previous values, showing a steady decline from 6 R_J outward. The Galileo data show no evidence of the "impoundment ramp" observed in the Voyager data [*Bagenal and Sullivan*, 1981].

The Galileo plasma data presented in this paper are all available online, and any data not already in the Planetary Data System will be submitted shortly. It will be interesting to compare the plasma properties presented here with those measured by NASA's Juno mission after orbit insertion (4 July 2016) and by future JUICE and Europa missions.

Appendix A: Data Analysis Method

A1. Data Collection and Instrument Response

The PLS data were returned in four different modes with four different accumulation times, with separate data records for the odd- and even-numbered anodes. The four modes are easiest to understand graphically as shown in Figure A1. Mode 1 returns data from just the lowest 16 channels and is not used in the current analysis. Mode 2 is a low-resolution mode that returns every fourth energy channel with an accumulation time of 0.5 s per energy step. However, each record is either the top or bottom half of the range (see Figure A1). Mode 3 is a medium-resolution mode that returns every third channel with an accumulation time of 0.2667 s per energy step; again, each record is either the top or bottom half (see Figure A1). In order to build up a complete merged array for Modes 2 and 3 requires collecting separate records for both the top and bottom halves, for both the odd and even anodes. Mode 4 is a high-resolution mode with an accumulation time of 0.15 s whereby all channels between 12 and 63 are covered via four energy sweeps that step through every fourth channel in each sweep, for both the odd and even anodes. After a complicated merging process (see supporting information) the net result is a set of energy-time spectra for each of seven anodes in a set of directions per spin of the spacecraft. Further details are provided in the supporting information. Each anode has an effective area for collecting the ion flux as a function of energy. The values of the geometric factors are given in the supporting information.

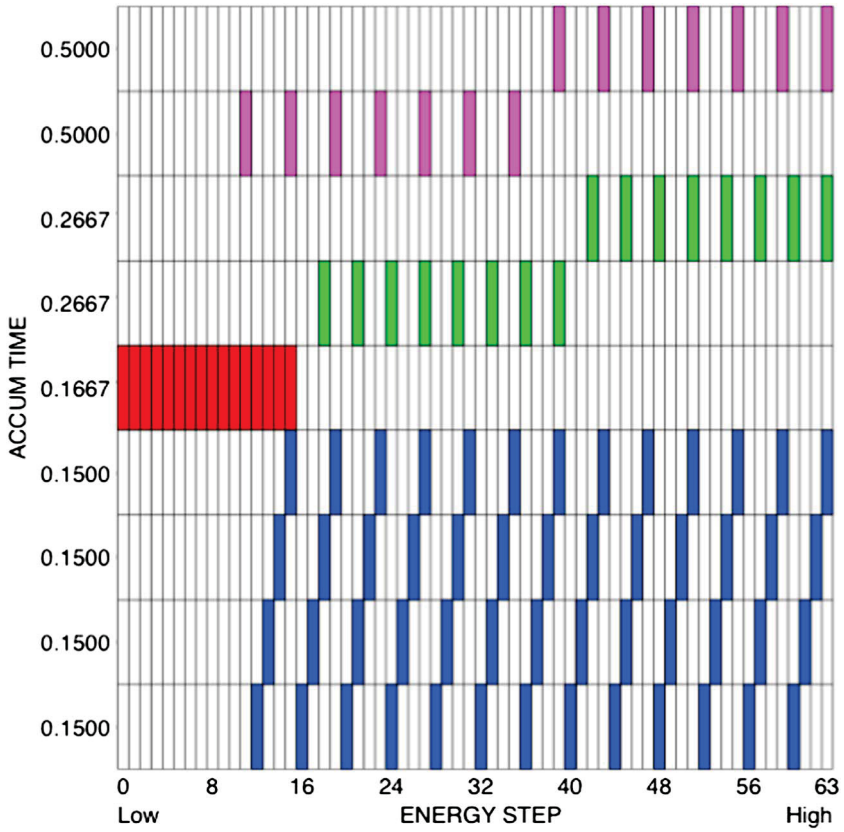

Figure A1. The four different accumulation times of PLS data: Modes 1–4, are shown in red, magenta, green, and blue, respectively.

A2. Fitting Procedure

To derive plasma parameters of density, isotropic temperature, and a velocity vector, a forward model of a single ion species three-dimensional Maxwellian distribution was employed. We used the best calibration values available (and sometimes previously unpublished) for PLS's energy tables, geometric factors/efficiencies, and look directions. The single ion species was assumed with a specified mass and charge, both varying with radial distance, based on the findings of *Delamere et al*. [2005]. Much preprocessing of the individual data was required to collect merged arrays suitable, rejecting intervals where there is insufficient signal. Likewise, much postpruning of fits was carried out to remove unphysical results. There were cases of too little signal above the noise level or the plasma environment changing faster than the merged array cadence (as we have to assume, plasma conditions are constant over the interval of data we fit). The remaining data used for this study have uncertainties of $<$100% on density, temperature, and V_ϕ; exclude data from within $10\,R_{moon}$ during any moon flyby; and are within $30\,R_J$. Full details of the method and calibrations used for fitting and pruning can be found in the extensive supporting information accompanying this article.

In Figure A2 we show a couple examples of merged array energy spectra for low-resolution (0.5 s accumulation time) data at two different times. We picked two locations, both about $15\,R_J$ from the planet, on the dawnside and duskside of the magnetosphere. The four rows are the four quadrants of a spin as defined by Sector ID, merging both the upper and lower "flavors" of the low-resolution, and odd and even spins, with counts per accumulation of all seven anodes (A1 to A7). The data are not shown for anodes at background levels. The raw unmerged spectrograms for these intervals are shown in Figure S4 in the supporting information. The dash-dotted line shows the Maxwellian function that has been fit to the spectra where the anodes exhibit significant counts. This highlights the fact that the signal is generally only found in one anode or two anodes and for just one or two azimuths. The limited amount of clear signal indicates the difficulty in deriving

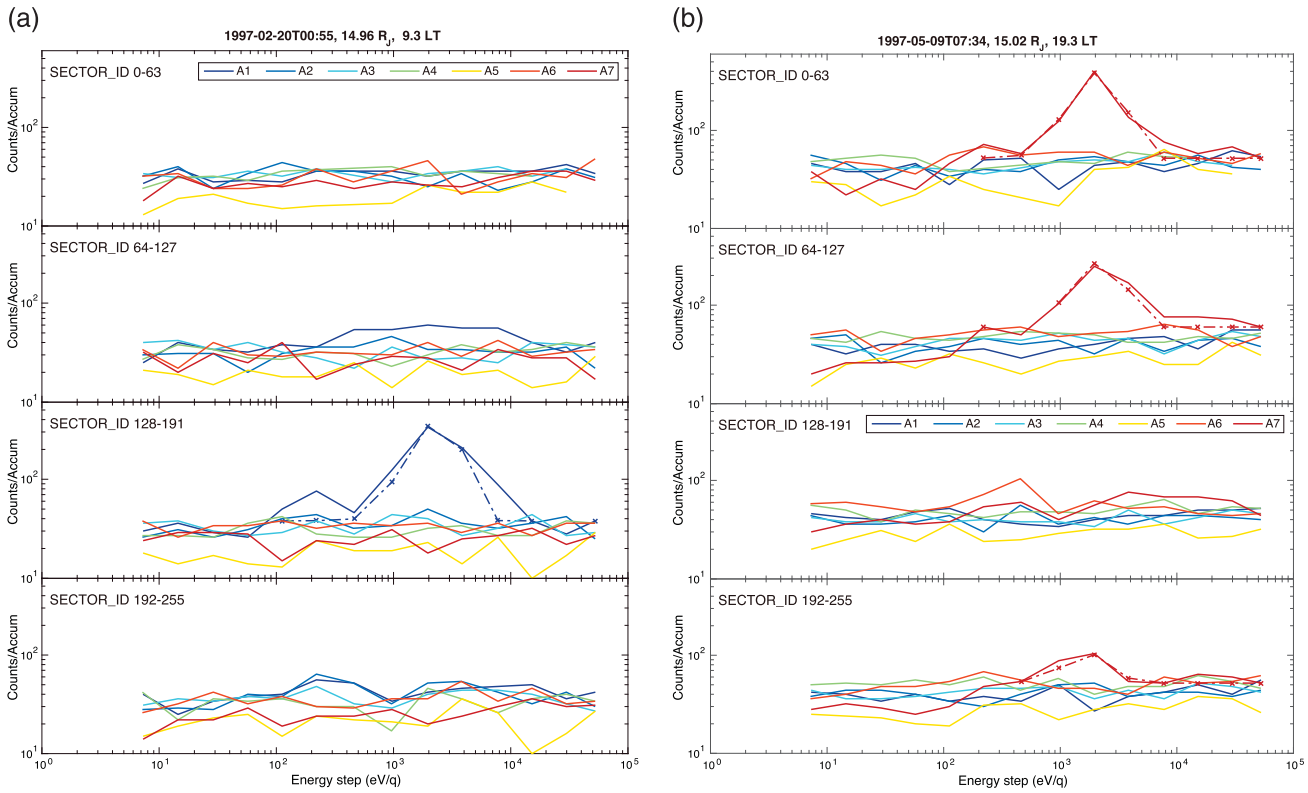

Figure A2. (a) Example of merged-spin spectra for low-resolution (0.5 s accumulation time) data obtained on 20 February 1997 at 14.96 R_J around dawn local time (LT). The four rows are the four quadrants of a spin as defined by Sector ID, merging both the upper and lower flavors of the low-resolution, and odd and even spins, with counts per accumulation of all seven anodes (A1 to A7). The dash-dotted line shows the fitted Maxwellian for these shapes for the peak anodes (not shown for anodes at background). (b) Same as Figure A2a but for 9 May 1997 at 15.02 R_J on the duskside.

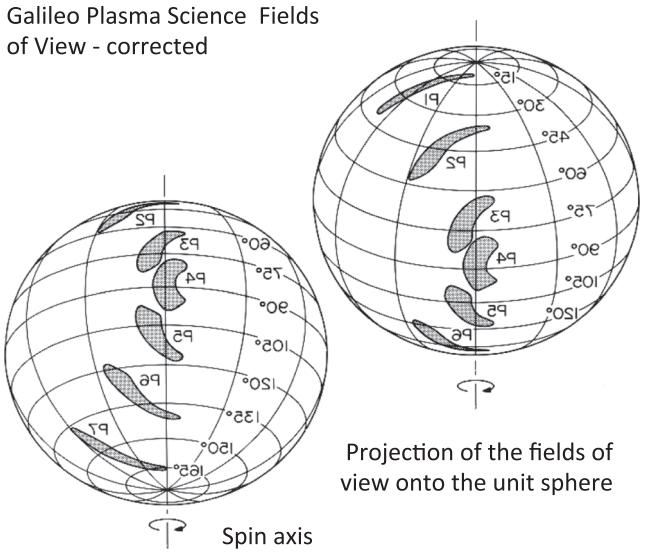

Figure A3. Fields of view of the seven different anodes of the Galileo PLS instrument. Note that the writing is shown backward because of the flipping of the orientation of the coordinate system relative to the originally published figure in *Frank et al.* [1992].

full plasma parameters from these data. In particular, any small variations around the main azimuthal flow direction are poorly determined.

A3. Coordinate Transformations

The Galileo mission predated the widespread use of NASA's NAIF Spice kernels and uses Rotor Right Ascension, Rotor Declination, Rotor Twist, and Rotor Spin to give position and orientation information of Galileo, while the PLS data records provide a value that can be used for spin phase. The Rotor values are all in EME-50 coordinates except Rotor Spin that is in ECL-50 coordinates. It is vital not to assume that all four are EME-50 coordinates, otherwise the fitted parameters are likely to produce artificial local time dependence.

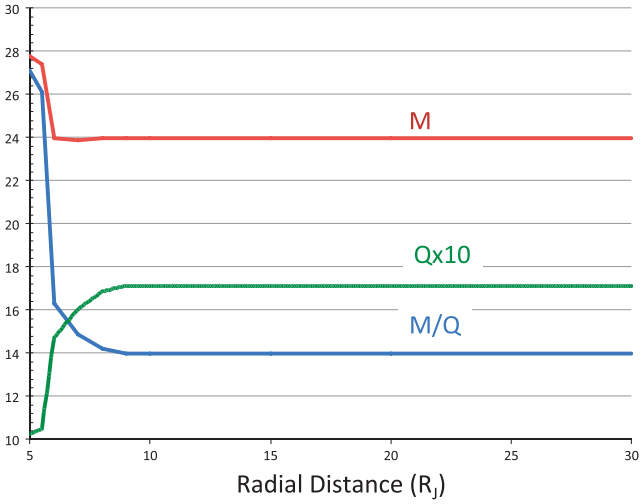

Figure A4. Composition as a function of radial distance. The derived average mass (*M* in atomic mass units), charge state (*Q*), and *M*/*Q* are shown, based on physical chemistry model of *Delamere et al.* [2005]. This radial profile of composition was used in forward fitting Galileo PLS data.

See the supporting information for the full discussion of this issue.

The spin phase from PLS data records must be used to correctly assign spin phase rather than utilizing the record time stamps. PLS record time stamps have uncertainties of several seconds and are the times the data were stored on board and not the time the data were taken. The spin phase value (SECTOR_ID in the PLS file) is the onboard measured spin phase as the data were taken.

A figure showing locations of the anodes and Galileo spin direction was provided in the PLS instrument paper [*Frank et al.*, 1992], but it was incorrect. Later *Paterson* [2009] improved the figure, but it needs further correction (as described in the supporting information). Figure A3 shows the corrected figure as validated by comparison with observed PLS data.

A4. Composition

The most complete observations of ion composition are provided by the EUV emissions of the Io plasma torus. These emissions have been matched by models of physical chemistry of the neutral-plasma system. The low spectral resolution and low Mach number of the flows means that the heavy ions (O^{++}, S^{+++}, O^{+}, S^{++}, and S^{+}) tend to overlap in the energy-per-charge spectrum. It is particularly frustrating that the dominant ions O^{+} and S^{++} have the same mass-to-charge ratio of 16. We have therefore assumed a certain average mass-to-charge ratio and fit each spectrum with a single heavy ion species. Figure A4 is a plot of composition versus distance based on a physical chemistry model of the torus [*Delamere et al.*, 2005] that is constrained by Cassini UVIS observations. We also show in Figure A4 radial profiles of average ion mass (A_i or *M* in atomic mass unit), average ion charge state (Z_i or *Q*), and average mass-to-charge ratio *M*/*Q* (amu/e).

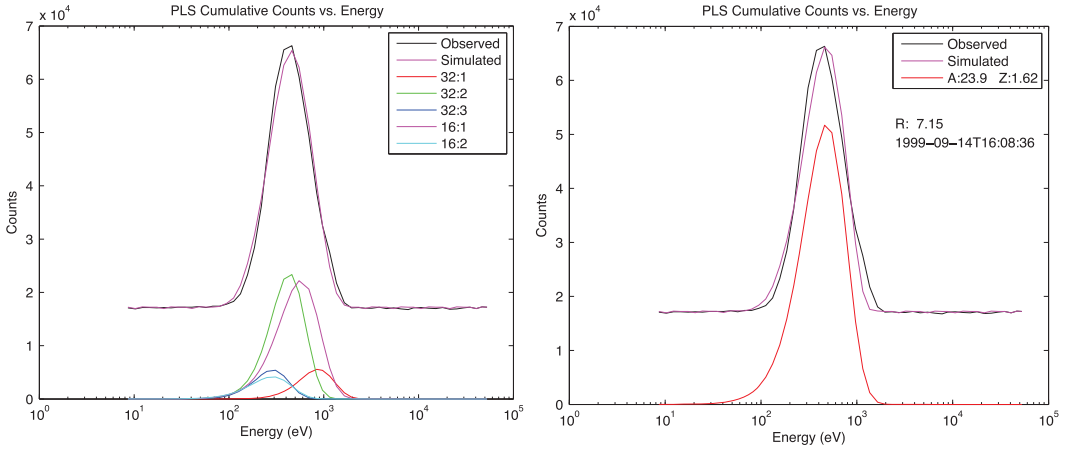

Figure A5. Fits for single species and multiple species—comparison suggests that ion temperature derived from fitting a single species over estimates the ion temperature by a factor of about 1.4.

Table A1. Comparison of Bulk Plasma Parameters Derived by Fitting the PLS Spectrum in Figure A5 With Single and Multiple Ion Species

	Multispecies	Single Species
$N_i/\Sigma N_i$	$O^{++} = 0.11$ $S^{+++} = 0.11$ $S^{++} = 0.34$ $O^{+} = 0.41$ $S^{+} = 0.064$	M = 23.9 Q = 1.64 M/Q = 14.6
Ne (cm^{-3})	387	376
Ti (eV)	121	168
V_ϕ (km/s)	74	73

A5. Temperature Factor

With limited resolution of the energy-per-charge spectrum and the generally transonic flow of the ions, the separate peaks of the multiple ion species corotating with Jupiter merge together into a single peak. Figure A5 shows a sample comparison of counts versus energy profiles. Figure A5 (right) shows the observed data (black) and the best fit data generated by the model using a single species Maxwellian function for all the heavy ions. Figure A5 (left) shows this information for when all five of the dominant species in the Io torus were included (assumed to share the same temperature) with prescribed ion mixing ratios from the physical chemistry model of *Delamere et al*. [2005]. The resulting densities, temperatures, and azimuthal speeds from these fits are shown in Table A1. We explored how changing the composition (±2 in the value of *M*, ±0.2 in *Q*) impacts the derived parameters. We found that density is the most sensitive changing by 25%, with the effects changing *M* and *Q* anticorrelated. Changing *M* and *Q* was also anticorrelated for V_ϕ but at the 7% level. The ion temperature was insensitive to changes in *M* and changed by 5% with a ±0.2 change in *Q*.

We carried out this exercise at several distances and found that the mix of multiple ions matches the data with a cooler temperature—by a factor of 1.4—than the single ion peak. We have therefore divided the ion temperature derived by fitting the energy-per-charge spectrum with a single heavy ion species by a factor of 1.4 to compensate for not including multiple ions.

Acknowledgments

We acknowledge support from NASA's Jupiter Data Analysis Program (NNX09AE03G). The Galileo PLS instrument is described at this website: http://www-pi.physics.uiowa.edu/pls/ The University of Iowa subnode of PDS for Planetary Plasma Interactions is provided here: http://www-pw.physics.uiowa.edu/pds/home.html The Galileo PLS plasma data used in the forward model plasma parameters calculations came from volume GO-J-PLS-3-RDR-FULLRES-V1.0 in the Planetary Data System (PDS) at http://pds.nasa.gov/. Likewise, the plasma numerical moments from the Galileo PLS instrument are found in the GO-J-PLS-5-RTS-MOMENTS-V1.0 PDS volume. The data used in this analysis, the supporting information describing the analysis techniques, the plasma moments derived from different techniques, and the *Paterson* [2009] document are all presented at this website: http://lasp.colorado.edu/home/mop/missions/galileo-2/galileo-plasma-data-pls/.

References

Bagenal, F. (1994), Empirical model of the Io plasma torus: Voyager measurements, *J. Geophys. Res.*, *99*, 11,043–11,062, doi:10.1029/93JA02908.

Bagenal, F., and P. A. Delamere (2011), Flow of mass and energy in the magnetospheres of Jupiter and Saturn, *J. Geophys. Res.*, *116*, A05209, doi:10.1029/2010JA016294.

Bagenal, F., and J. D. Sullivan (1981), Direct plasma measurements in the Io torus and inner magnetosphere of Jupiter, *J. Geophys. Res.*, *86*, 8447–8466, doi:10.1029/JA086iA10p08447.

Bagenal, F., F. J. Crary, A. I. F. Stewart, N. M. Schneider, D. A. Gurnett, W. S. Kurth, L. A. Frank, and W. R. Paterson (1997), Galileo measurements of plasma density in the Io torus, *Geophys. Res. Lett.*, *24*, 2119–2122, doi:10.1029/97GL01254.

Bagenal, F., T. Dowling, and W. McKinnon (2004), Introduction, in *Jupiter: Planet, Satellites, Magnetosphere*, edited by F. Bagenal, T. Dowling, and W. McKinnon, 719 pp., Cambridge Univ. Press, Cambridge, U. K.

Bagenal, F., et al. (2014), Magnetospheric science objectives of the Juno mission, *Space Sci. Rev.*, doi:10.1007/s11214-014-0036-8.

Bagenal, F., E. Sidrow, R. J. Wilson, T. A. Cassidy, V. Dols, F. J. Crary, A. J. Steffl, P. A. Delamere, W. S. Kurth, and W. R. Paterson (2015), Plasma conditions at Europa's orbit, *Icarus*, *261*, 1–13.

Barnhart, B. L., W. S. Kurth, J. B. Groene, J. B. Faden, O. Santolik, and D. A. Gurnett (2009), Electron densities in Jupiter's outer magnetosphere determined from Voyager 1 and 2 plasma wave spectra, *J. Geophys. Res.*, *114*, A05218, doi:10.1029/2009JA014069.

Crary, F. J., F. Bagenal, J. A. Ansher, D. A. Gurnett, and W. S. Kurth (1996), Anisotropy and proton density in the Io plasma torus, *J. Geophys. Res.*, *101*, 2699–2706, doi:10.1029/95JA02212.

Crary, F. J., F. Bagenal, L. A. Frank, and W. R. Paterson (1998), Galileo Plasma Spectrometer Measurements of Composition and Temperature in the Io Plasma Torus, *J. Geophys. Res.*, *103*, 29,359–29,370, doi:10.1029/1998JA900003.

D'Amario, L. A., L. E. Bright, and A. A. Wolf (1992), Galileo Trajectory Design, *Space Sci. Rev.*, *60*, 23–78.

Delamere, P. A., and F. Bagenal (2003), Modeling variability of plasma conditions in the Io torus, *J. Geophys. Res.*, *108*(A7), 1276, doi:10.1029/2002JA009706.

Delamere, P. A., A. Steffl, and F. Bagenal (2004), Modeling temporal variability of plasma conditions in the Io torus during the Cassini era, *J. Geophys. Res.*, *109*, A10216, doi:10.1029/2003JA010354.

Delamere, P. A., F. Bagenal, and A. Steffl (2005), Radial variations in the Io plasma torus during the Cassini era, *J. Geophys. Res.*, *110*, A12223, doi:10.1029/2005JA011251.

Dols, V., P. A. Delamere, F. Bagenal, W. S. Kurth, and W. R. Paterson (2012), Asymmetry of Io's outer atmosphere: Constraints from five Galileo flybys, *J. Geophys. Res.*, *117*, E10010, doi:10.1029/2012JE004076.

Frank, L. A., and W. R. Paterson (1999a), Production of Hydrogen Ions at Io, *J. Geophys. Res.*, *104*, 10,345–10,354, doi:10.1029/1999JA900052.

Frank, L. A., and W. R. Paterson (1999b), Intense electron beams observed at Io with the Galileo spacecraft, *J. Geophys. Res.*, *104*, 28,657–28,669, doi:10.1029/1999JA900402.

Frank, L. A., and W. R. Paterson (2000a), Observations of plasmas in the Io torus with the Galileo spacecraft, *J. Geophys. Res.*, *105*, 16,017–16,034, doi:10.1029/1999JA000250.

Frank, L. A., and W. R. Paterson (2000b), Return to Io by the Galileo spacecraft: Plasma observations, *J. Geophys. Res.*, *105*, 25,363–25,378, doi:10.1029/1999JA000460.

Frank, L. A., and W. R. Paterson (2001a), Survey of thermal ions in the Io plasma torus with the Galileo spacecraft, *J. Geophys. Res.*, *106*, 6131–6149, doi:10.1029/2000JA000159.
Frank, L. A., and W. R. Paterson (2001b), Passage through Io's ionospheric plasmas by the Galileo spacecraft, *J. Geophys. Res.*, *106*, 26,209–26,224, doi:10.1029/2000JA002503.
Frank, L. A., and W. R. Paterson (2002a), Plasmas observed with the Galileo spacecraft during its flyby over Io's northern polar region, *J. Geophys. Res.*, *107*(A8), 1220, doi:10.1029/2002JA009240.
Frank, L. A., and W. R. Paterson (2002b), Galileo observations of electron beams and thermal ions in Jupiter's magnetosphere and their relationship to the auroras, *J. Geophys. Res.*, *107*(A12), 1478, doi:10.1029/2001JA009150.
Frank, L. A., and W. R. Paterson (2004), Plasmas observed near local noon in Jupiter's magnetosphere with the Galileo spacecraft, *J. Geophys. Res.*, *109*, A11217, doi:10.1029/2002JA009795.
Frank, L. A., K. L. Ackerson, J. A. Lee, M. R. English, and G. L. Pickett (1992), The plasma instrumentation for the Galileo mission, *Space Sci. Rev.*, *60*, 283–307.
Frank, L. A., W. R. Paterson, K. L. Ackerson, V. M. Vasyliunas, F. V. Coroniti, and S. J. Bolton (1996), Plasma observations at Io with the Galileo Spacecraft, *Science*, *274*, 394–395.
Frank, L. A., W. R. Paterson, and K. K. Khurana (2002), Observations of thermal plasmas in Jupiter's magnetotail, *J. Geophys. Res.*, *107*(A1), 1003, doi:10.1029/2001JA000077.
Gurnett, D. A., W. S. Kurth, R. R. Shaw, A. Roux, R. Gendrin, C. F. Kennel, F. L. Scarf, and S. D. Shawhan (1992), The Galileo plasma wave investigation, *Space Sci. Rev.*, *60*, 341–355.
Gurnett, D. A., W. S. Kurth, A. Roux, S. J. Bolton, and C. F. Kennel (1996), Galileo plasma wave observations in the Io plasma torus and near Io, *Science*, *274*, 391–392.
Gurnett, D. A., W. S. Kurth, A. Roux, S. J. Bolton, E. A. Thomsen, and J. B. Green (1998), Galileo plasma wave observations near Europa, *Geophys. Res. Lett.*, *25*, 237–240, doi:10.1029/97GL03706.
Gurnett, D. A., A. M. Persoon, W. S. Kurth, A. Roux, and S. J. Bolton (2000), Plasma densities in the vicinity of Callisto from Galileo plasma wave observations, *Geophys. Res. Lett.*, *27*(13), 1867–1870, doi:10.1029/2000GL003751.
Gurnett, D. A., A. Persoon, and W. Kurth (2001), Electron densities near Io from Galileo plasma wave observations, *J. Geophys. Res.*, *106*, 26,225–26,232, doi:10.1029/2000JA002509.
Herbert, F., N. M. Schneider, and A. J. Dessler (2008), New description of Io's cold plasma torus, *J. Geophys. Res.*, *113*, A01208, doi:10.1029/2007JA012555.
Hess, S. L. G., P. A. Delamere, F. Bagenal, N. Schneider, and A. J. Steffl (2011), Longitudinal modulation of hot electrons in the Io plasma torus, *J. Geophys. Res.*, *116*, A11215, doi:10.1029/2011JA016918.
Hill, T. (1976), Interchange stability of a rapidly rotating magnetosphere, *Planet. Space Sci.*, *24*, 1151–1154.
Hill, T. W., and F. C. Michel (1976), Heavy ions from the Galilean satellites and the centrifugal distortion of the Jovian magnetosphere, *J. Geophys. Res.*, *81*, 4561–4565, doi:10.1029/JA081i025p04561.
Johnson, T. V., C. M. Yeates, and R. Young (1992), Galileo mission overview, *Space Sci. Rev.*, *60*, 3–21.
Khurana, K., M. G. Kivelson, V. Vasyliunas, N. Krupp, J. Woch, A. Lagg, B. Mauk, and W. Kurth (2004), The configuration of Jupiter's magnetosphere, in *Jupiter: Planet, Satellites, Magnetosphere*, edited by F. Bagenal, T. Dowling, and W. McKinnon, pp. 593–616, Cambridge Univ. Press, Cambridge, U. K.
Kivelson, M. G., K. K. Khurana, C. T. Russell, and R. J. Walker (1997), Intermittent short-duration plasma-field anomalies in the Io plasma torus: Evidence for interchange in the Io plasma torus?, *Geophys. Res. Lett.*, *24*, 2127, doi:10.1029/97GL02202.
Krupp, N., A. Lagg, S. Livi, B. Wilken, J. Woch, E. C. Roelof, and D. J. Williams (2001a), Global flows of energetic ions in Jupiter's equatorial plane: First-order approximation, *J. Geophys. Res.*, *106*, 26,017–26,032, doi:10.1029/2000JA900138.
Krupp, N., J. Woch, A. Lagg, E. C. Roelof, D. J. Williams, S. Livi, and B. Wilken (2001b), Local time asymmetry of energetic ion anisotropies in the Jovian magnetosphere, *Planet. Space Sci.*, *49*, 283–289.
Krupp, N., et al. (2004), Dynamics of the Jovian magnetosphere, in *Jupiter: Planet, Satellites, Magnetosphere*, edited by F. Bagenal, T. E. Dowling, and W. B. McKinnon, pp. 617–638, Cambridge Univ. Press, Cambridge, U. K.
Kurth, W. S., D. A. Gurnett, A. M. Persoon, A. Roux, S. J. Bolton, and C. J. Alexander (2001), The plasma wave environment of Europa, *Planet. Space Sci.*, *49*, 345–363.
Lellouch, E., M. A. McGrath, and K. L. Jessup (2007), Io's atmosphere, in *Io After Galileo*, edited by R. M. C. Lopes and J. R. Spencer, pp. 231–264, Springer, Praxis.
Lellouch, E., M. Ali-Dib, K.-L. Jessup, A. Smette, H.-U. Käufl, and F. Marchis (2015), Detection and characterization of Io's atmosphere from high-resolution 4-lm spectroscopy, *Icarus*, *253*, 99–114.
McNutt, R. L., J. W. Belcher, and H. S. Bridge (1981), Positive ion observations in the middle magnetosphere of Jupiter, *J. Geophys. Res.*, *86*, 8319–8342, doi:10.1029/JA086iA10p08319.
Paterson, W. R. (2009), Refinement of plasma measurements from the Galileo mission to Jupiter, NASA JDAP Grant NNG05GJ23G final report.
Paterson, W. R., L. A. Frank, and K. L. Ackerson (1999), Galileo plasma observations at Europa: Ion energy spectra and moments, *J. Geophys. Res.*, *104*, 22,779–22,791, doi:10.1029/1999JA900191.
Rathbun, J. A., and J. R. Spencer (2010), Ground-based observations of time variability in multiple active volcanoes on Io, *Icarus*, *209*, 625–630.
Steffl, A. J., F. Bagenal, and A. I. F. Stewart (2004), Cassini UVIS observations of the Io plasma torus. II: Radial variations, *Icarus*, *172*, 91–103.
Steffl, A. J., P. A. Delamere, and F. Bagenal (2006), Cassini UVIS observations of the Io plasma torus. III. Modeling temporal and azimuthal variability, *Icarus*, *180*, 124–140, doi:10.1016/j.icarus.2005.07.013.
Steffl, A. J., P. A. Delamere, and F. Bagenal (2008), Cassini UVIS observations of the Io plasma torus. IV. Observations of temporal and azimuthal variability, *Icarus*, *194*, 153–165, doi:10.1016/j.icarus.2007.09.019.
Thomas, N., F. Bagenal, T. Hill, and J. Wilson (2004), The Io neutral clouds and plasma torus, in *Jupiter: Planet, Satellites, Magnetosphere*, edited by F. Bagenal, T. E. Dowling, and W. B. McKinnon, pp. 561–592, Cambridge Univ. Press, Cambridge, U. K.
Thorne, R. M., T. P. Armstrong, S. Stone, D. J. Williams, R. W. McEntire, S. J. Bolton, D. A. Gurnett, and M. G. Kivelson (1997), Galileo evidence for rapid interchange transport in the Io torus, *Geophys. Res. Lett.*, *24*, 2131–2134, doi:10.1029/97GL01788.
Tokar, R. L., D. A. Gurnett, and F. Bagenal (1982), The proton concentration in the vicinity of the Io plasma torus, *J. Geophys. Res.*, *87*, 10,395–10,400, doi:10.1029/JA087iA12p10395.
Tsang, C. C., J. R. Spencer, E. Lellouch, M. A. Lopez-Valverde, M. J. Richter, and T. K. Greathouse (2012), Io's atmosphere: Constraints on sublimation support from density variations on seasonal timescales using NASA IRTF/TEXES observations from 2001 to 2010, *Icarus*, *217*, 277–296.

Tsang, C. C., J. R. Spencer, and K. L. Jessup (2015), Non-detection of post-eclipse changes in Io's Jupiter-facing atmosphere: Evidence for volcanic support?, *Icarus*, *248*, 243–253.

Vasyliunas, V. M., L. A. Frank, K. L. Ackerson, and W. R. Paterson (1997), Geometry of the plasma sheet in the midnight-to-dawn sector of the Jovian magnetosphere: Plasma observations with the Galileo spacecraft, *Geophys. Res. Lett.*, *24*, 869–872, doi:10.1029/97GL00757.

Wang, K., R. M. Thorne, R. B. Horne, and W. S. Kurth (1998a), Cold torus whistlers: An indirect probe of the inner Jovian plasmasphere, *J. Geophys. Res.*, *103*, 14,987–14,994, doi:10.1029/98JA00965.

Wang, K., R. M. Thorne, R. B. Horne, and W. S. Kurth (1998b), Constraints on Jovian plasma properties from a dispersion analysis of unducted whistlers in the warm Io torus, *J. Geophys. Res.*, *103*, 14,979–14,986, doi:10.1029/98JA00964.

Wilson, R. J. (2015), Error analysis for numerical estimates of space plasma parameters, *Earth Space Sci.*, *2*, 201–222, doi:10.1002/2014EA000090.

Woch, J., N. Krupp, and A. Lagg (2002), Particle bursts in the Jovian magnetosphere: Evidence for a near-Jupiter neutral line, *Geophys. Res. Lett.*, *29*(7), 1138, doi:10.1029/2001GL014080.

Yoshikawa, I., et al. (2014), Extreme ultraviolet radiation measurement for planetary atmospheres/magnetospheres from the Earth-orbiting spacecraft (Extreme Ultraviolet Spectroscope for Exospheric Dynamics: EXCEED), *Space Sci. Rev.*, *184*, 237–258.

Yoshioka, K., G. Murakami, A. Yamazaki, F. Tsuchiya, M. Kagitani, T. Sakanoi, T. Kimura, K. Uji, and I. Yoshikawa (2013), The Extreme Ultraviolet Spectroscope for Planetary Science, EXCEED, *Planet. Space Sci.*, *85*, 250–260.

Zarka, P., J. Queinnec, and F. J. Crary (2001), Low-frequency limit of Jovian radio emissions and implications on source locations and Io plasma wake, *Planet. Space Sci.*, *49*, 1137–1149.